Title: Antimicrobial wound care in an ant society

Authors: Erik. T. Frank[1,2]*, Lucie Kesner[3], Joanito Liberti[1,3], Quentin Helleu[1,4], Adria C. LeBoeuf[5], Andrei Dascalu[1], Douglas B. Sponsler[2], Fumika Azuma[6], Evan P. Economo[6,7], Patrice Waridel[8], Philipp Engel[3], Thomas Schmitt[2], Laurent Keller[1]

Affiliations:

[1]Department of Ecology and Evolution, Biophore, University of Lausanne; CH-1015 Lausanne, Switzerland.

[2]Department of Animal Ecology and Tropical Biology, Biocenter, University of Würzburg; D-97074 Würzburg, Germany.

[3]Department of Fundamental Microbiology, Biophore, University of Lausanne; CH-1015 Lausanne, Switzerland.

[4]Structure et Instabilité des Génomes, Muséum National d'Histoire Naturelle, CNRS UMR 7196, INSERM U1154, 43 rue Cuvier, F-75005 Paris, France

[5]Department of Biology, University of Fribourg; CH-1700 Fribourg, Switzerland.

[6]Biodiversity and Biocomplexity Unit, Okinawa Institute of Science & Technology Graduate University; Onna, 904-0495, Japan.

[7]Radcliffe Institute for Advanced Study, Harvard University, Cambridge, 02138, USA.

[8]Protein Analysis Facility, Génopode, University of Lausanne; CH-1015 Lausanne, Switzerland.

*Corresponding author. Email: erik.frank@uni-wuerzburg.de

Infected wounds pose a major mortality risk in animals[1,2]. Injuries are common in the ant *Megaponera analis,* which raids pugnacious prey[3,4]. Here we show that *M. analis* can determine when wounds are infected and treat them accordingly. By applying a variety of antimicrobial compounds and proteins secreted from the metapleural gland to infected wounds, workers reduce the mortality of infected individuals by 90%. Chemical analyses showed that wound infection is associated with specific changes in the cuticular hydrocarbon profile, thereby likely allowing nestmates to diagnose the infection state of injured individuals and apply the appropriate antimicrobial treatment. This study demonstrates that the targeted use of antimicrobials to treat infected wounds, previously thought to be a uniquely human behavior, has evolved in insect societies as well.

Infected wounds are a major mortality risk for animals[1,2], but the identification and medicinal treatment of infected wounds has thus far been considered a uniquely human behavior. While several mammals have been shown to lick wounds and apply saliva[1,2], the efficacy of this behavior remains largely unknown and occurs irrespective of the state of the wound. Workers of the predatory ant *Megaponera analis* have been shown to care for the injuries of nestmates[3,4], which are common because this ant feeds exclusively on pugnacious termite species. As many as 22% of the foragers engaging in raids attacking termites have one or two missing legs[3]. Injured workers are carried back to the nest where other workers treat their wounds[4]. When the

wounds of injured workers are not treated by nestmates, 90% of the injured workers die within 24 hours after injury[4], but the mechanisms behind these treatments are unknown.

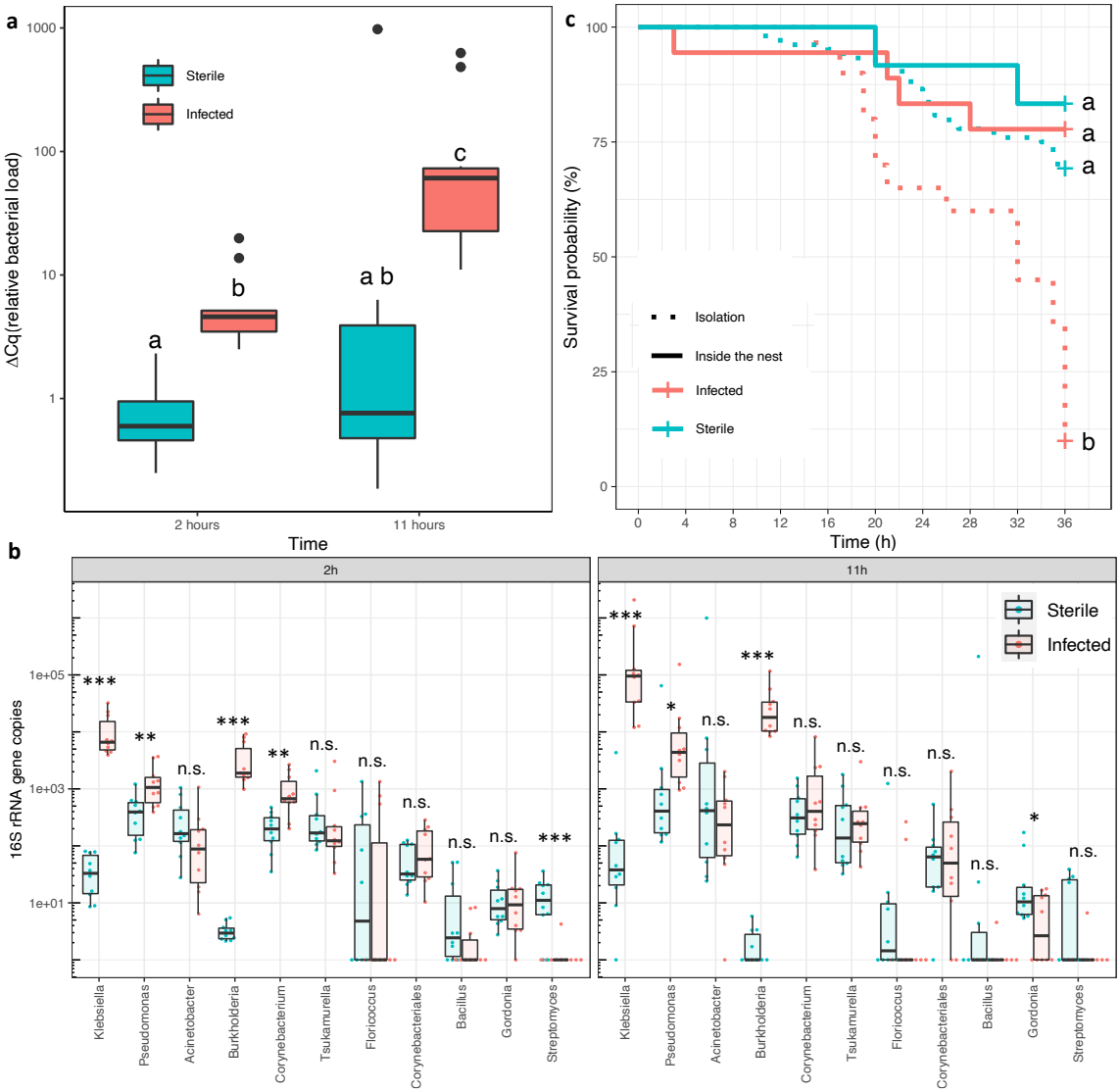

Fig. 1 | Lethal effects and diversity of soil pathogens. (a) Relative 16S rRNA gene copies (bacterial load ΔCq) for individuals whose wounds were exposed to a sterile PBS solution (Sterile), or soil pathogens diluted in PBS (Infected, OD=0.1), 2 and 11 hours after exposure (see Supplemental Table 1 for statistical results). *n*=10 per boxplot. Significant differences (*P*<0.05) are shown with different letters. **(b)** Absolute 16S rRNA gene copy numbers summarized at the genus-level for the 18 amplicon sequence variants (ASV) that had at least 1% relative abundance in five of the 40 analyzed ants across the experiment (*n*=10 per boxplot). Significance is shown for pairwise comparisons between sterile and infected ants: ***=*P*<0.001; **=*P*<0.01; *=*P*<0.05; n.s.= not significant (*P*>0.05). Detailed statistical results in Supplemental Table 2 **(c)** Kaplan – Meier cumulative survival rates of workers in isolation (dotted line) or inside the nest (solid line) whose wounds were exposed the same way as in Fig. 1a (infected or sterile). Significant differences (*P*<0.05) are indicated with different letters (detailed statistical results in Extended Data Fig. 2a and Supplemental Table 3).

To investigate whether the high mortality of injured individuals is due to infection by pathogens, we collected soil from the natural environment and applied it to the wounds of experimentally injured workers (i.e., a sterile cut in the middle of the femur on the hind leg of

an otherwise healthy ant). After 2 hours, injured ants exposed to the soil (hereafter referred to as "infected ants") had ten times higher bacterial loads in the thorax than similarly injured individuals exposed to sterile phosphate buffered saline (PBS, hereafter referred to as "sterile ants"; least square means: t=-3.08; P=0.01; Fig. 1a, Supplemental Table 1). After 11 hours, bacterial load further increased in infected ants (least square means: t=-3.66; P=0.003), while there was no such increase in sterile ants (least square means: t=-1.54; P=0.26; Fig. 1a). As a result, after 11 hours the bacterial load was 100 times higher in infected than sterile ants (least square means: t=-5.21; P<0.001; Fig. 1a). A microbiome analysis further revealed major differences in bacterial species composition and abundance between the two groups of ants (ADONIS: F=17.45; R^2=0.31; P<0.001; Fig. 1b & Extended Data Fig. 1a, b), with three potentially pathogenic bacterial genera increasing in absolute abundance in the thorax of infected ants at both time-points: *Klebsiella*, *Pseudomonas* and *Burkholderia* (Fig. 1b, Supplemental Table 2). These differences in bacterial composition and abundance between infected and sterile ants were associated with important differences in survival probability, with survival being seven times lower for infected ants (least square means: Z=-4.246; P<0.001; Fig. 1c, Extended Data Fig. 2a & Supplemental Table 3).

To test if wound care by nestmates could reduce the mortality of infected ants, we either placed infected and sterile ants in their colony or kept them in isolation. The mortality after 36 hours was much lower for infected ants kept with their nestmates (22%) than for infected ants kept in isolation (90%, least square means: Z=-2.759; P=0.02; Fig. 1c). By contrast, there was no significant difference between the mortality of sterile ants kept with their nestmates or in isolation (least square means: Z=1.04; P=0.89; Fig. 1c). The mortality of infected ants was also not significantly different than the mortality of sterile ants when these individuals were kept with their nestmates (least square means: Z=-0.630; P=1; Fig. 1c). Overall, these data demonstrate that *M. analis* workers are capable of effectively treating wounds that have been exposed to soil pathogens.

By culturing the soil medium on agar plates, we were able to isolate three potential pathogens (the endosymbiotic bacterium *Burkholderia* sp. and its fungal host *Rhizopus microsporus*, and the bacterium *Pseudomonas aeruginosa*, Fig. 1b, Extended Data Fig. 1c, d). While the application of *B.* sp. and *R. microsporus* (separately or together) on wounds did not significantly decrease survival (Extended Data Fig. 2b & 3), the application of *P. aeruginosa* (OD=0.05), a bacterium widespread in various environments[5], caused a mortality of 93%

within 36 hours (Fig. 2a). Since the treatment with only *P. aeruginosa* showed a similar mortality as the treatment with all soil pathogens (90%, Extended Data Fig. 3), we only used *P. aeruginosa* in subsequent infection assays to better control pathogen load.

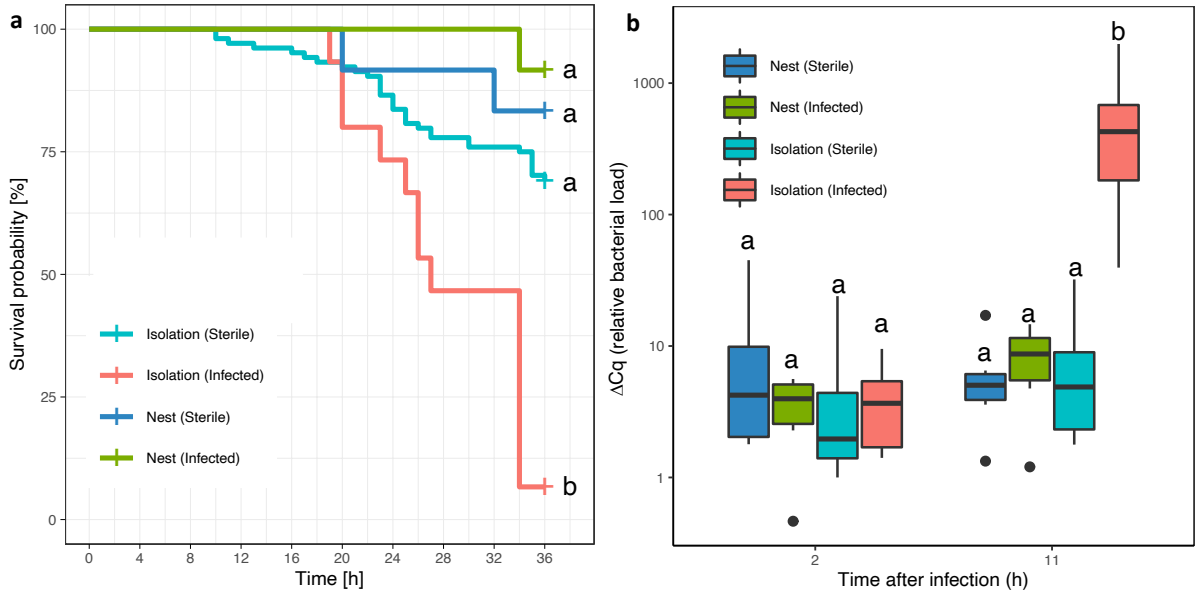

Fig. 2 | Survival probability and pathogen load of sterile and infected ants. (a) Kaplan – Meier cumulative survival rates of workers in isolation (dotted line) or inside the nest (solid line) whose wounds were exposed to *P. aeruginosa* diluted in PBS (Infected, OD=0.05) or a sterile PBS solution (Sterile). Detailed statistical results in Extended Data Fig. 2c and Supplemental Table 3. **(b)** relative bacterial load (ΔCq) of *Pseudomonas* at two different time points (2h and 11h) for ants in isolation or inside the nest with wounds treated the same way as in Fig. 2a (Infected or Sterile). *n*=6 per boxplot, significant differences (*P*<0.05) are shown with different letters (Supplemental Table 4).

Like the experiments where the soil was applied to the wound, the presence of nestmates was also effective in decreasing the mortality of injured workers exposed to a known concentration of *P. aeruginosa* (OD=0.05). While the mortality of infected ants kept in isolation was 93%, mortality of infected ants that had been returned to their nestmates was only 8% (least square means: *Z*=-2.94; *P*=0.01; Fig. 2a, Extended Data Fig. 2c & Supplemental Table 4). There were major differences in the increase in *Pseudomonas* load after injury between ants kept with or without their nestmates (Fig. 2b & Supplemental Table 5). The bacterial load of infected ants kept with their nestmates did not increase significantly from 2 and 11 hours after injury (least square means: *t*=-0.037, *P*=1; Fig. 2b). By contrast, there was a 100-fold increase in bacterial load for infected ants kept in isolation (least square means: *t*=-4.832, *P*<0.001; Fig. 2b).

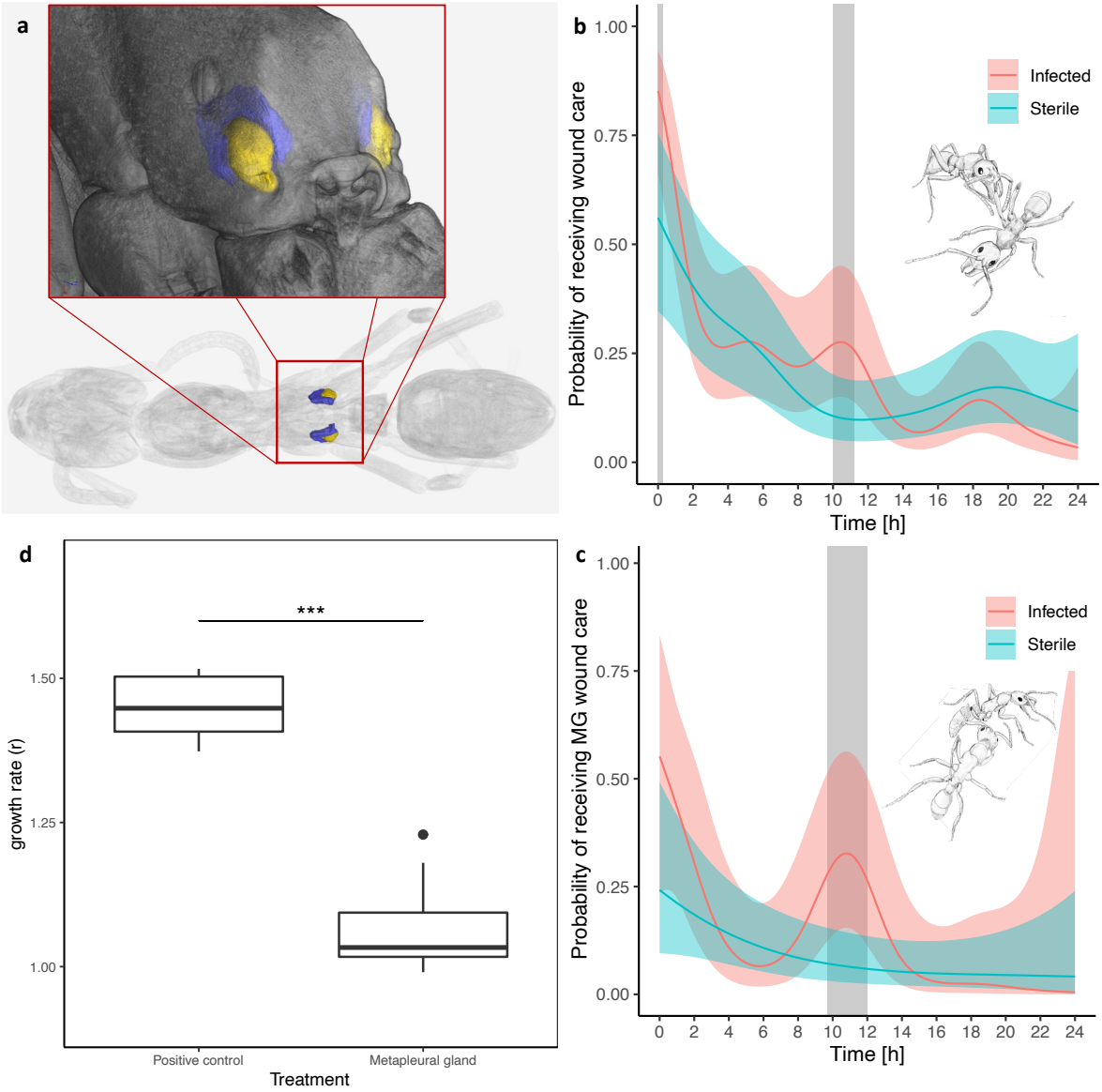

Fig. 3 | Use and efficacy of the metapleural gland (MG) secretions during wound care. (a) Micro CT scan showing the location of the MG. Blue: secretory cells; yellow: atrium. **(b)** Probability of receiving wound care over 24 hours fitted with a hierarchical generalized (binomial) additive model (HGAM); shaded bars indicate periods during which the probability of receiving care was significantly ($P<0.05$) higher for infected (n=6) than sterile (n=6) individuals. **(c)** Probability of receiving antimicrobial wound care with MG secretions (the same ants as in Fig. 3b), modeled with identical HGAM specifications. **(d)** Bacterial growth assay for *P. aeruginosa* either in LB broth (positive control, n=6) or LB broth with MG secretions (Metapleural gland n=9). Mann-Whitney U test: W=54, P<0.001.

To study the proximate mechanisms reducing mortality of infected ants when they are returned to their nestmates, we introduced injured ants (with sterile and infected wounds) to their nestmates and filmed them for 24 hours. We observed that workers treated the injury of infected ants by depositing secretions produced by the metapleural gland (MG), which is located at the back of the thorax (Fig. 3a). The MG secretions, which have antimicrobial properties[6-10], were applied in 10.5% of the wound care interactions (43 out of 411). Before applying MG

129 secretions, the nursing ant always groomed the wound first (i.e., "licking" the wound with their
130 mouthparts). Nursing ants then collected the secretions either from their own MGs
131 (Supplemental Movie 1), by reaching back to the opening of the gland with their front legs to
132 collect the secretion and then licking their front legs to accumulate it in their mouth, as
133 described in other species[8], or from the MG of the injured ant itself, by licking directly into the
134 gland's opening (Supplemental Movie 2). Wound care with MG secretions lasted significantly
135 longer (85±53s) than wound care without MG secretions (53±36s; t-test: t=-3.09, P=0.003;
136 Extended Data Fig. 4). Remarkably, workers were able to discriminate between infected and
137 sterile ants. Wound care treatment was provided more often to infected ants upon initial
138 introduction to the nest and again 10- and 11-hours post-introduction (hierarchical generalized
139 additive model: P<0.05; Fig. 3b). Moreover, MG secretions were deposited significantly more
140 often on wounds of infected than sterile ants between 10 and 12 hours after infection
141 (hierarchical generalized additive model: P<0.05; Fig. 3c). When treatment with MG secretions
142 was prevented (through plugging the MG opening of all ants in the sub-colony), mortality of
143 infected ants reached 100% within 36h compared to only 33% when workers had access to the
144 MG secretions (least square means: Z=2.99; P=0.039; Fig. 4; Extended Data Fig. 5 &
145 Supplemental Table 6). By contrast, the plugging of the MG opening had no significant effect
146 on the survival of sterile ants (least square means: Z=0.02; P=1; Fig. 4, fig. S5 & table S6).
147
148 Because cuticular hydrocarbons (CHCs) are known to be frequently used as a source of
149 information in ants[11], we investigated whether infected ants could signal their injured state
150 through changes in the profile. Immediately after injury, infected ants did not differ from sterile
151 ants in their CHC profile (ADONIS: R^2=0.13; F=0.13; P=0.96; Supplemental Table 7 & 8).
152 This profile changed in both types of ants during the two hours after injury (Sterile ants:
153 ADONIS: R^2=0.15; F=2.74; P=0.03; Infected ants: ADONIS: R^2=0.13; F=2.42; P=0.05),
154 converging towards a similar profile for both types of ants (ADONIS: R^2=0.008; F=0.17;
155 P=0.87). Thereafter, the CHC profile of infected ants remained unchanged until 11 hours after
156 injury (ADONIS: R^2=0.063; F=1.48; P=0.13), while the CHC profile of sterile ants changed
157 significantly (ADONIS: R^2=0.14; F=3.54; P=0.04), thereby becoming significantly different
158 from the CHC profile of infected ants (ADONIS: R^2=0.19; F=5.4; P=0.007). Eleven hours after
159 injury, the CHC profile of sterile ants had converged again to the profile at 0h (ADONIS:
160 R^2=0.03; F=0.53; P=0.45), while the CHC profile of injured ants remained significantly
161 different (ADONIS: R^2=0.19; F=3.82; P=0.008).
162

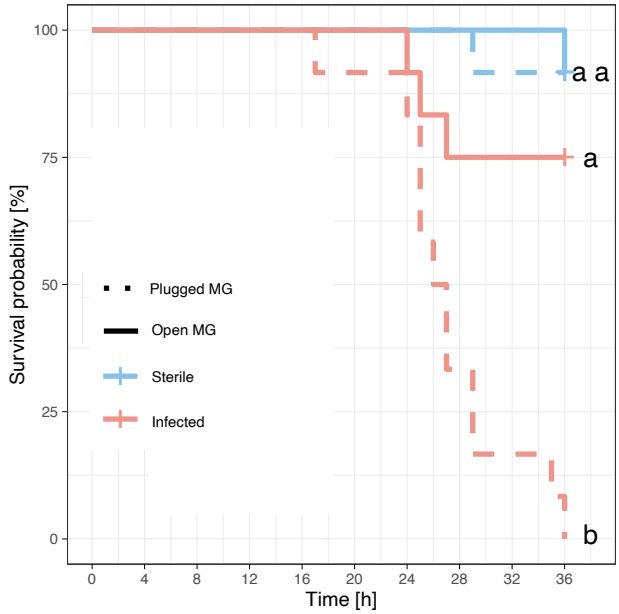

Fig. 4 | Effect of MG secretions on survival of sterile and infected ants. Kaplan – Meier cumulative survival rates of workers inside sub-colonies with a plugged MG opening (dotted line) or with an unmanipulated MG opening (solid line) whose wounds were exposed to a sterile PBS solution (Sterile *n*=12) or *P. aeruginosa* diluted (OD=0.05) in PBS (Infected *n*=12). Detailed statistical results in Extended Data Fig. 2d and Supplemental Table 5. Data for ants in isolation in Extended Data Fig 5.

Consistent with the idea that changes in CHC profiles could provide information on the health status of ants[12], the observed differences in the CHC profiles mostly stemmed from differences in the relative abundance of alkadienes (Extended Data Fig. 6, Supplemental Table 9), which are among the CHC compounds most relevant for communication in social insects[13]. These changes in the CHC profile are generally regulated by differentially expressed genes in the fat body[14]. To identify the genes likely responsible for the observed CHC changes between infected and sterile ants, we conducted transcriptomic analyses of the fat bodies of the same individuals. A total of 18 genes related to CHC synthesis were differentially expressed between infected and sterile ants 11 hours after exposure to *P. aeruginosa* (17 genes out of 378 that were differentially expressed were immune genes; Extended Data Fig. 7a, Supplemental Table 10 & 11), while only two genes related to CHC synthesis were differentially expressed two hours after infection (in addition to 7 immune genes out of 164; Extended Data Fig. 6b, Supplemental Table 10 & 11).

To quantify the capabilities of MG secretions to inhibit bacterial growth, we conducted antimicrobial assays. The growth of *P. aeruginosa* was reduced by >25% when MG secretions were included in a lysogeny broth (LB) solution compared to a control LB solution without the MG secretions (Mann-Whitney U test: W=54, P<0.001, Fig. 3d).

188 Since *P. aeruginosa* has repeatedly developed antimicrobial resistance[15] and because most
189 antimicrobial compounds found in animal saliva are unable to inhibit the growth of *P.*
190 *aeruginosa*[16], we conducted proteomic and chemical analyses of the MG secretions. The
191 proteomic analysis revealed 41 proteins (Extended Data Fig. 8 & Supplemental Table 12), 15
192 of which showed molecular similarity to toxins, which often have antimicrobial properties[17].
193 Five proteins had orthologs known to have antimicrobial activity (e.g., lysozyme, hemocytes,
194 2 MRJP1-like proteins) and three with melanization, a process implicated in wound healing in
195 insects[18,19]. There was no clear function for nine proteins including the most abundant protein
196 (13±16% of the MG's endogenous protein content), for which no ortholog could be found. The
197 evolutionarily young gene coding this protein could be a promising candidate for antimicrobial
198 research, with research into next-generation antibiotics often relying on antimicrobial
199 peptides[20]. The gas-chromatography/mass-spectrometry (GC-MS) analyses of the MG further
200 revealed 112 organic compounds (23 of which could not be identified, Extended Data Fig. 9,
201 Supplemental Table 13). Six of the identified compounds had antibiotic- and/or fungicide-like
202 structures and 35 were alkaloids. While we could not identify the exact structure of the
203 alkaloids, many of them are known to have antimicrobial properties[21]. There were also 14
204 carboxylic acids, making up 52% of the secretions content (Extended Data Fig. 9,
205 Supplemental Table 13), probably leading to a lower pH detrimental to bacterial survival and
206 growth[6].
207
208 The number of chemical compounds identified in the MG's secretions of *M. analis* (112) is far
209 greater than in other ant species, where the number of compounds ranges between 1 and 35 and
210 mostly consists of carboxylic acids rather than alkaloids or antibiotic-like compounds[6]. While
211 MG secretions have been observed to be used to sterilize the nest or as a response to fungal
212 exposure in other ant species[6,8,10], it had never been observed in the context of wound care.
213 During wound care, the use of the MG secretions probably fulfils a similar role as the
214 mammals' antiseptic saliva. This analogous role likely led to the convergent evolution of
215 functionally similar antimicrobial and wound healing proteins[22]. However, this treatment is
216 indiscriminate in mammals as it has never been observed to depend on the infected state of the
217 wound.
218
219 This study reveals a highly effective behavioral adaptation to identify and treat festering
220 infections of open wounds in a social insect. The prophylactic and therapeutic use of
221 antimicrobial secretions to counteract infection in *M. analis* (Fig. 3c) mirrors modern medical

222 procedures used for treating dirty wounds[23]. Remarkably, the primary pathogen in ant's
223 wounds, *Pseudomonas aeruginosa*, is also a leading cause of infection in combat wounds,
224 where infections can account for 45% of casualties in humans[24]. This demonstrates
225 convergence in both the challenges of warfare and the solutions that evolved to mediate them
226 in human and insect societies.

227 **References**

228 1. Hart, B.L. Behavioural defences in animals against pathogens and parasites: parallels with the pillars of
229 medicine in humans. *Phil Trans R Soc B* **366**, 3406-3417 (2011).
230 2. Kessler, S.E. Why Care: Complex Evolutionary History of Human Healthcare Networks. *Frontiers in*
231 *psychology* **11**, 199 (2020).
232 3. Frank, E.T. *et al.*, Saving the injured: Rescue behavior in the termite hunting ant *Megaponera analis*.
233 *Science Advances* **3**, e1602187 (2017).
234 4. Frank, E.T., Wehrhahn, M. & Linsenmair, K.E. Wound treatment and selective help in a termite-
235 hunting ant. *Proc R Soc B* **285**, 20172457 (2018).
236 5. Diggle, S.P. & Whiteley, M. Microbe Profile: *Pseudomonas aeruginosa*: opportunistic pathogen and
237 lab rat. *Microbiology* **166**, 30-33 (2020).
238 6. Yek, S.H. & Mueller, U.G. The metapleural gland of ants. *Biol Rev* **86**, 774-791 (2011).
239 7. Fernandez-Marin, H. *et al.*, Functional role of phenylacetic acid from metapleural gland secretions in
240 controlling fungal pathogens in evolutionarily derived leaf-cutting ants. *Proc R Soc B* **282**, 20150212
241 (2015).
242 8. Fernandez-Marin, H., Zimmerman, J. K., Rehner, S. A. & Wcislo, W. T. Active use of the metapleural
243 glands by ants in controlling fungal infection. *Proc R Soc B* **273**, 1689-1695 (2006).
244 9. Tranter, C., Fernandez-Marin, H. & Hughes, W. O. H. Quality and quantity: transitions in antimicrobial
245 gland use for parasite defense. *Ecol Evol* **5**, 857-868 (2015).
246 10. Yek, S. H., Nash, D. R., Jensen, A. B. & Boomsma, J. J. Regulation and specificity of antifungal
247 metapleural gland secretion in leaf-cutting ants. *Proc R Soc B* **279**, 4215-4222 (2012).
248 11. Leonhardt, S. D., Menzel, F., Nehring, V. & Schmitt, T. Ecology and Evolution of Communication in
249 Social Insects. *Cell* **164**, 1277-1287 (2016).
250 12. Pull, C.D. *et al.*, Destructive disinfection of infected brood prevents systemic disease spread in ant
251 colonies. *Elife* **7**, e32073 (2018).
252 13. Drijfhout, F., Kather, R. & Martin, S. "The role of cuticular hydrocarbons in insects" in *Behavioral and*
253 *Chemical Ecology,* W. Zhan, H. Liu, Eds. (Nova Science Pub Inc, 2009), chap. 3.
254 14. Holze, H., Schrader, L. & Buellesbach, J. Advances in deciphering the genetic basis of insect cuticular
255 hydrocarbon biosynthesis and variation. *Heredity* **126**, 219-234 (2021).
256 15. Poole, K. Efflux-mediated multiresistance in Gram-negative bacteria. *Clin Microbiol Infec* **10**, 12-26
257 (2004).
258 16. Hart, B. L. & Powell, K. L. Antibacterial Properties of Saliva - Role in Maternal Periparturient
259 Grooming and in Licking Wounds. *Physiol Behav* **48**, 383-386 (1990).
260 17. Primon-Barros, M. & Macedo, A. J. Animal Venom Peptides: Potential for New Antimicrobial Agents.
261 *Curr Top Med Chem* **17**, 1119-1156 (2017).
262 18. Janusz, G. *et al.*, Laccase Properties, Physiological Functions, and Evolution. *Int J Mol Sci* **21**, 966
263 (2020).
264 19. Yang, W.J. *et al.*, Single Amino Acid Substitution in Homogentisate Dioxygenase Affects Melanin
265 Production in *Bacillus thuringiensis*. *Front Microbiol* **9**, 2242 (2018).
266 20. Moretta, A. *et al.*, Antimicrobial Peptides: A New Hope in Biomedical and Pharmaceutical Fields.
267 *Front Cell Infect Microbiol* **11**, 668632 (2021).
268 21. Cushnie, T.P.T., Cushnie, B. & Lamb, A. J., Alkaloids: An overview of their antibacterial, antibiotic-
269 enhancing and antivirulence activities. *Int J Antimicrob Ag* **44**, 377-386 (2014).
270 22. Vila, T., Rizk, A. M., Sultan, A. S. & Jabra-Rizk, M. A. The power of saliva: Antimicrobial and
271 beyond. *Plos Pathog* **15**, e1008058 (2019).
272 23. Leaper, D. J. Prophylactic and Therapeutic Role of Antibiotics in Wound Care. *Am J Surg* **167**, 15-20
273 (1994).
274 24. Bobrov, A. G. *et al.*, Evaluation of *Pseudomonas aeruginosa* pathogenesis and therapeutics in military-
275 relevant animal infection models. *Apmis*, (2021).

Figure Legends

Fig. 1 | Lethal effects and diversity of soil pathogens. (a) Relative 16S rRNA gene copies (bacterial load ΔCq) for individuals whose wounds were exposed to a sterile PBS solution (Sterile), or soil pathogens diluted in PBS (Infected, OD=0.1), 2 and 11 hours after exposure (see Supplemental Table 1 for statistical results). *n*=10 per boxplot. Significant differences (*P*<0.05) are shown with different letters. **(b)** Absolute 16S rRNA gene copy numbers summarized at the genus-level for the 18 amplicon sequence variants (ASV) that had at least 1% relative abundance in five of the 40 analyzed ants across the experiment (*n*=10 per boxplot). Significance is shown for pairwise comparisons between sterile and infected ants: ***=*P*<0.001; **=*P*<0.01; *=*P*<0.05; n.s.= not significant (*P*>0.05). Detailed statistical results in Supplemental Table 2 **(c)** Kaplan – Meier cumulative survival rates of workers in isolation (dotted line) or inside the nest (solid line) whose wounds were exposed the same way as in Fig. 1a (infected or sterile). Significant differences (*P*<0.05) are indicated with different letters (detailed statistical results in Extended Data Fig. 2a and Supplemental Table 3).

Fig. 2 | Survival probability and pathogen load of sterile and infected ants. (a) Kaplan – Meier cumulative survival rates of workers in isolation (dotted line) or inside the nest (solid line) whose wounds were exposed to *P. aeruginosa* diluted in PBS (Infected, OD=0.05) or a sterile PBS solution (Sterile). Detailed statistical results in Extended Data Fig. 2c and Supplemental Table 3. **(b)** relative bacterial load (ΔCq) of *Pseudomonas* at two different time points (2h and 11h) for ants in isolation or inside the nest with wounds treated the same way as in Fig. 2a (Infected or Sterile). *n*=6 per boxplot, significant differences (*P*<0.05) are shown with different letters (Supplemental Table 4).

Fig. 3 | Use and efficacy of the metapleural gland (MG) secretions during wound care. (a) Micro CT scan showing the location of the MG. Blue: secretory cells; yellow: atrium. **(b)** Probability of receiving wound care over 24 hours fitted with a hierarchical generalized (binomial) additive model (HGAM); shaded bars indicate periods during which the probability of receiving care was significantly (P<0.05) higher for infected (n=6) than sterile (n=6) individuals. **(c)** Probability of receiving antimicrobial wound care with MG secretions (the same ants as in Fig. 3b), modeled with identical HGAM specifications. **(d)** Bacterial growth assay for *P. aeruginosa* either in LB broth (positive control, *n*=6) or LB broth with MG secretions (Metapleural gland *n*=9). Mann-Whitney U test: *W*=54, *P*<0.001.

Fig. 4 | Effect of MG secretions on survival of sterile and infected ants. Kaplan – Meier cumulative survival rates of workers inside sub-colonies with a plugged MG opening (dotted line) or with an unmanipulated MG opening (solid line) whose wounds were exposed to a sterile PBS solution (Sterile *n*=12) or *P. aeruginosa* diluted (OD=0.05) in PBS (Infected *n*=12). Detailed statistical results in Extended Data Fig. 2d and Supplemental Table 5. Data for ants in isolation in Extended Data Fig 5.

310 # Methods

311 **Experimental design**

312 The study was conducted in a humid savannah woodland located in the Comoé National Park,
313 northern Côte d'Ivoire (Ivory Coast), at the Comoé National Park Research Station (8°46'N,
314 3°47'W)[25]. Experiments, observations, and sample collections in the Comoé National Park
315 were carried out from April to June 2018, February, April to June and September to October
316 2019, April 2020 and October 2022. *Megaponera analis* is found throughout sub-Saharan
317 Africa from 25°S to 12°N[26] and known to show monophasic allometry within its worker sizes[27].
318 We thus divided the workers into majors (head width > than 2.40 mm), minors (head width <
319 1.99 mm) and intermediates (head width 2.40 - 1.99 mm). All experiments were carried out on
320 the minor caste, the individuals most frequently injured[3]. All field studies were conducted in
321 accordance with local legislation and permission by the Office Ivoirien des Parcs et Réserves
322 (OIPR).

323 **Laboratory colonies**

324 Eleven colonies, including queen and brood (colony size 1083±258 ants), were excavated and
325 placed in artificial nests in the field stations laboratory. PVC nests (30x20x10 cm) were
326 connected to a 1x1m feeding arena. The ground surface was covered with soil from the
327 surrounding area (up to a height of 2 cm). Colonies were fed by placing in the feeding arena
328 *Macrotermes bellicosus* termites collected from the surrounding area. These termites were
329 found by scouts and triggered raiding behavior. The laboratory windows were kept open to
330 maintain a natural humidity, temperature, and day-night cycle (light regime).

331 **Survival of injured ants**

332 To quantify the lethality of various types of pathogens, workers were injured by a sterile cut in
333 the middle of the femur on the hind leg and had the fresh wound submerged for 2 seconds in a
334 10 µL phosphate buffered saline (PBS) solution with a known pathogen concentration (approx.
335 10^6 bacteria). Afterwards the injured ants were placed inside a cylindrical glass container with
336 a diameter of 3 cm and a height of 5 cm. Before the experiments, the glass containers were
337 filled with 1 cm of surface soil and placed for 3 hours at 220 °C in an oven together with the
338 forceps and scissors for sterilization. Nest-like humidity was created by moistening the soil
339 with 1 mL of sterilized water (boiled for ten minutes) and covered with aluminum foil. The
340 isolation experiments were conducted at 24°C in a sterile room. To test for mortality, the
341 injured ant was checked upon once per hour for the next 36 hours, if no reaction was observed

342 even after shaking the container the ant was classified as dead. To ensure replicability of the
343 survival experiments a negative (sterile PBS solution) and positive control (using a sterile PBS
344 solution with 0.1 optical density (OD) of *Pseudomonas aeruginosa* (PSE)) were always
345 included during each survival experiment. The sample sizes were PBS: *n*=104; PSE 0.1: *n*=61;
346 PSE 0.05: n=15 (Fig. 2a & Extended Data Fig. 3). For all sample sizes and statistics see
347 Extended Data Fig. 2.

348 To test if wound care by nestmates reduces the mortality of infected ants, we first marked 10
349 ants per colony during a raid. 24 hours later, all marked ants were injured in the same way as
350 in the isolation trial. Afterwards, the wound of the injured ant was either exposed to a sterile
351 PBS solution (sterile), a sterile PBS solution containing 0.05 OD of *P. aeruginosa* or a sterile
352 PBS solution containing 0.1 OD of surface soil pathogens (grown on agar plates). Isolation
353 trials with the same treatments were always conducted in parallel. Sample size of in nest
354 survival experiments: PBS: *n*=12; PSE 0.05: *n*=12; Soil *n*=18 (Fig. 1c & 2a). For all sample
355 sizes and statistics see Extended Data Fig. 2.

356 To test the importance of the Metapleural gland (MG) secretions we divided three colonies
357 (approx. 1000 ants) into two equally sized sub-colonies including brood. The queens were left
358 with a small retinue of 20 workers in a separate container. For each colony we plugged the MG
359 opening of all workers of one of the sub-colonies with acrylic color, while for the other sub-
360 colony acrylic color was placed on the thorax of the workers. Afterwards the experimental
361 procedure was identical to the wound care experiment described above. Eight individuals were
362 removed from each sub-colony, marked, and wounded and the wound exposed to either a sterile
363 PBS solution (*n*=4 per sub-colony) or a sterile PBS solution containing 0.05 OD of *P.*
364 *aeruginosa* (*n*=4 per sub-colony). Sample sizes were thus in total: Sterile: *n*=12; Infected: *n*=12
365 for both treatments (with and without plugged MG opening; Fig. 4). In addition, to quantify
366 any effects of the plugging of the MG opening on individuals, a parallel experiment with *n*=12
367 Sterile and *n*=12 Infected ants with or without plugged MG opening was run in isolation
368 (Extended Data fig. 5 & Supplemental Table 6).

369 The pathogen concentration was measured by optical density (OD) using a portable Ultrospec
370 10 cell density meter (Biochrom) with sterile PBS as solvent. For the soil pathogens, we
371 collected surface soil in the surrounding area of the nest and grew it over 36 hours on agar
372 plates (Extended Data Fig. 1b). For *P. aeruginosa* we created cultures of the isolated strains
373 (Extended Data fig. 1c) in the field lab from frozen samples kept in Tryptic Soy Broth (TSB)
374 medium with 25% glycerol (stored and transported at -23°C). After replating the bacterial

375 culture once on a fresh plate, we waited 16 hours before applying the pathogen on fresh
376 wounds. For all experiments, we used trypticase soy agar (TSA) plates to culture the bacteria.

377 **Treatment of wounds by nestmates**

378 To quantify the wound care behaviors inside the nest, we filmed the ants using a Panasonic
379 HC-X1000 and analyzed the videos using VLC media player v.3.0.16 Vetinari (intel 64bit).
380 The wound of the injured ant was either exposed to a sterile PBS solution (Sterile) or a sterile
381 PBS solution containing 0.05 OD of *P. aeruginosa* (Infected).

382 All manipulated ants were placed in front of the nest entrance directly after a raid and the nest
383 was filmed for the subsequent 24 hours. Only one trial was conducted per colony with a total
384 of four injured ants per colony (two sterile and two infected), in a total of three colonies (i.e.,
385 *n*=6 infected ants and *n*=6 sterile ants, Fig. 3b, c). The observed wound care behaviors were
386 classified into two categories: (1) wound care: a nestmate cleans the open wound with its
387 mouthparts; (2) metapleural gland (MG) care: a nestmate collects MG secretions either from
388 its own gland (Supplemental Movie 1) or from the injured ant (Supplemental Movie 2) in its
389 mouth before caring for the wound. These behaviors were quantified for the first 24 hours and
390 summarized in 10 min intervals.

391 **Sample collection protocol for chemical, genetic and microbial analyses**

392 To quantify the cuticular hydrocarbon (CHC) profile, differential gene expression (Extended
393 Data Fig. 6) and pathogen load in the thorax content (Fig. 1a & 2b), we used the same
394 experimental design as used to quantify the survival of injured ants (see above). In total, 30
395 sterile and 30 infected ants (*P. aeruginosa* OD=0.05) were prepared, 12 sterile and 12 infected
396 ants were kept in isolation, another 12 sterile and infected ants were placed inside the nest and
397 6 sterile and 6 infected ants were collected immediately after injury. Sterile or infected ants
398 were then collected from their enclosures at either 2 or 11 hours after manipulation (*n*=6 per
399 treatment). Only ants that did not die until these time points were used for further analyses. The
400 collected ants were then first placed in hexane for 10 minutes to extract the CHC profile. The
401 gaster was then cut off and placed in RNAlater for genetic analyses and the thorax was placed
402 in 100% ethanol for the microbial analyses. The samples for genetic and microbial analyses
403 were brought to the University of Lausanne and the samples for chemical analyses to the
404 University of Würzburg. Another 10 sterile and 10 infected ants kept in isolation were further
405 observed for a total of 36 hours to ensure that the survival curves in this experiment resembled
406 those in Fig. 2a.

407 **Pathogen identification & isolation**

408 To isolate potential pathogens, we collected surface soil in the surrounding area of the nest and
409 grew its water extract on Sarborough Dextrose Agar (SDA) plates for 36 h at local temperature
410 to get the 'soil pathogen mix' (Extended Data Fig. 1b). Most of the plate was at first overgrown
411 by black mycelia identified as *Rhizopus microsporus.* This fungus is known to contain
412 symbiotic bacteria *Burkholderia* sp. (species not identified), as we confirmed by Sanger
413 sequencing and bacterial community analysis (Fig. 1b). After several days, the culture started
414 to show several large colonies of slimy microorganisms that were isolated and identified as
415 *Pseudomonas aeruginosa* (Extended Data Fig. 1c). For infection assays (Extended Data Fig.
416 3), we isolated *Burkholderia* and its fungal host *Rhizopus* from each other by repeated
417 passaging with antifungal nystatin (0.25 µl/ml in M9 agar, 30 °C) or antibacterial
418 ciprofloxamin (0.02 mg/ml in SDA). No representatives of *Klebsiella* were isolated.

419 The identification of all microorganisms was done by preparation of a PCR-ready DNA from
420 a piece of biomass as described in Lõoke et al.[28]. PCR reactions were done with universal
421 fungal primers ITS5 5'-TCCTCCGCTTATTGATATGC-3' and ITS4 5'-
422 GGAAGTAAAAGTCGTAACAAGG-3'[29] (GoTaq polymerase, Tm = 55 °C, elongation for
423 40 s) and commonly used universal bacterial primers 27F 5'-
424 AGRGTTYGATYMTGGCTCAG-3' and 1492R 5'-GGTTACCTTGTTACGACTT-3' (same
425 protocol but elongation for 1 min 20 s). The presence of PCR amplicons was verified on
426 electrophoresis gel and the fragments were sent for Sanger sequencing. Resulting sequences
427 were then screened against NCBI database with nucleotide BLAST[30].

428 **Microbiome analysis and bacterial load quantification**

429 To quantify the composition of the bacterial community in workers, we used the Powersoil
430 DNA isolation kit (MO Bio) to extract DNA from *M. analis* thoraxes kept in RNAlater.
431 Samples were homogenized by vortexing for 10 min, followed by two times 45 sec bead
432 beating at 6 m/s using a FastPrep24™ 5G homogenizer. Then we continued according to the
433 kit's manual and eluted DNA in 100 µL of nuclease-free water.

434 Bacterial loads were quantified with a QuantStudio5 qPCR instrument (Applied Biosystems)
435 using the reaction set up described in Kešnerová et al.[31] and the thermal cycling conditions
436 recommended for SYBR® Select Master Mix. For quantifying total bacterial loads, we used
437 our designed primers #1047 5'-AGGATTAGATACCCTRGTAGTC-3' and #1049 5'-
438 CATSMTCCACCRCTTGTGC-3' (at doubled 0.4 µM concentration). For specific targeting

439 we used *P. aeruginosa* primers #1209 5'-GTAGATATAGGAAGGAACACCAG-3' and
440 #1210 5'-GGTATCTAATCCTGTTTGCTCC-3' and for normalization to the host's
441 housekeeping gene we used *M. analis* 28S rRNA gene primers #1207 5'-
442 CTGCCCGGCGGTACTCG-3' and #1208 5'-ACCGGGGACGGCGCTAG-3'. Serial
443 dilutions (10x) showed that these primers performed with an amplification efficiency (E) of
444 1.86 (R^2= 0.99), 2.00 (R^2= 0.99), and 1.87 (R^2= 0.99), respectively.

445 Total bacterial (Fig. 1a) and *P. aeruginosa* (Fig. 2b) 16S rRNA gene (target) copy numbers
446 were expressed relatively to *M. analis* 28S rRNA gene copy numbers (host) based on the
447 following equation: $\Delta Cq = 2^{(Cq_{host} - Cq_{target})}$, where Cq was the measured 'quantification
448 cycle' value. To calculate the total 16S rRNA gene copy number in 1 µl of each DNA sample
449 that was used for absolute bacterial abundance based on ASV counts (Fig. 1b) we used the
450 equation n = E^(intercept – Cq)[32], where standard curve's *intercept* = 38.23[31].

451 **<u>16S rRNA gene amplicon-sequencing</u>**

452 16S rRNA gene amplicon sequencing data were obtained from 40 experimental samples, a
453 mock sample (to verify consistency of the MiSeq run compared to previous studies in our
454 group), two blank DNA extractions and a negative PCR control with only H_2O. We followed
455 the Illumina 16S metagenomic sequencing preparation guide
456 (https://support.illumina.com/documents/documentation/chemistry_documentation/16s/16s-
457 metagenomic-library-prep-guide-15044223-b.pdf) to amplify and sequence the V4 region of
458 the 16S rRNA gene. Primers for the first PCR step were 515F-Nex
459 (TCGTCGGCAGCGTCAGATGTGTATAAGAGACAGGTGCCAGCMGCCGCGGTAA)
460 and 806R-Nex
461 (GTCTCGTGGGCTCGGAGATGTGTATAAGAGACAGGGACTACHVGGGTWTCTAA
462 T). PCR amplifications were performed in a mix of 12.5 µL of Invitrogen Platinum SuperFi
463 DNA Polymerase Master Mix, 5 µL of MilliQ water, 2.5 µL of each primer (5 µM), and 2.5 µL
464 of template DNA. PCR conditions were 98 °C for 30 s, 25 cycles of 98 °C for 10 s, 55 °C for
465 20 s, and 72 °C for 20 s, and a final extension step at 72 °C for 5 min. Amplifications were
466 confirmed by 2% agarose gel electrophoresis. The PCR products were then purified with Clean
467 NGS purification beads (CleanNA) in a 1:0.8 ratio of PCR product to beads, and eluted in
468 27.5 µL of 10 mM Tris, pH 8.5. We then performed a second PCR step in which unique dual-
469 index combinations were appended to the amplicons using the Nextera XT index kit (Illumina).
470 Second-step PCRs were performed in a 25 µL, using 2.5 µL of the PCR products, 12.5 µL of
471 Invitrogen Platinum SuperFi DNA Polymerase Master Mix, 5 µL of MilliQ water, and 2.5 µL

472 of each of the Nextera XT indexing primers 1 and 2. PCR conditions were 95 °C for 3 min
473 followed by eight cycles of 30 s at 95 °C, 30 s at 55 °C, and 30 s at 72 °C, and a final extension
474 step at 72 °C for 5 min. The libraries were again purified using Clean NGS purification beads
475 in a 1:1.12 ratio of PCR product to beads, and eluted in 27.5 µL of 10 mM Tris, pH 8.5. The
476 amplicon concentrations, including the negative PCR control, mock and blanks, were
477 quantified by PicoGreen and pooled in equimolar concentrations (except for the water and
478 blank samples which were kept at lower concentrations). We verified that the final pool was of
479 the right size using a Fragment Analyzer (Advanced Analytical). MiSeq (Illumina) sequencing
480 was then performed at the Genomic Technology Facility of the University of Lausanne,
481 producing (2 × 250 bp) reads. We obtained a total of 979'126 paired-end reads across the 40
482 experimental samples.

483 **Analyses of 16 rRNA gene amplicon-sequencing data**

484 Raw sequencing data (deposited at the Sequence Read Archive (SRA) under PRJNA826317)
485 were analyzed with the Divisive Amplicon Denoising Algorithm 2 (DADA2) package v.1.20.0
486 in R. All functions were run using the recommended parameters
487 (https://benjjneb.github.io/dada2/tutorial.html) except for the filtering step in which we
488 truncated the forward and reverse reads after 232 and 231 bp, respectively. At the learnErrors
489 step, we then set randomize=TRUE and nbases=3e8. Amplicon-sequence variants (ASVs)
490 were classified with the SILVA database (version 138). Unclassified ASVs and any ASV
491 classified as chloroplast, mitochondria or Eukaryota were removed with the "phyloseq"
492 package version 1.36.0, using the "subset taxa" function. We then used the "prevalence"
493 method in the R package "decontam" v.1.12.0 to identify and remove contaminants introduced
494 during laboratory procedures, using the negative PCR control and the blank samples as
495 reference. This procedure filtered out three contaminant ASVs. Four additional ASVs were
496 removed as they clearly represented (low abundance) contaminants due to index swapping
497 from samples of a different project that were sequenced in the same sequencing run. We then
498 calculated absolute bacterial abundances of each ASV by multiplying the proportion of each
499 ASV by the total 16S rRNA gene copy number of each sample as measured by qPCR. To assess
500 differences in community structure between treatments we ran ADONIS tests after calculating
501 Bray-Curtis dissimilarities with the absolute ASV abundance matrix and plotted ordinations
502 based on these Bray-Curtis dissimilarities (Extended Data Fig. 1a).

503 To test for differences in absolute abundance of individual bacterial genera between sterile and
504 infected ants (Extended Data Fig. 1b), we used a permutation approach (permutation t-test) as

done in Kešnerová et al.[33]. To do this, we selected the ASVs that had at least 1% relative abundance across five samples (18 ASVs belonging to 11 genera). We then calculated copy numbers at the genus-level for each of the 40 samples. At each time-point (2 h and 11 h), we randomized the values of the calculated copy numbers for each genus 10,000 times and computed the *t* values for the tested effect for each randomized dataset. The *P* values corresponding to the effects were calculated as the proportion of 10,000 *t* values that were equal or higher than the observed one.

Chemical analysis of cuticular hydrocarbons

To quantify differences in CHC profiles between infected and sterile ant workers, cuticular hydrocarbon extracts were evaporated to a volume of approximately 100 µL and 1 µL was analyzed by using a 6890 gas chromatograph (GC) coupled to a 5975 mass selective detector (MS) by Agilent Technologies (Waldbronn, Germany). The GC was equipped with a DB-5 capillary column (0.25 mm ID × 30 m; film thickness 0.25 µm, J & W Scientific, Folsom, Ca, USA). Helium was used as a carrier gas with a constant flow of 1 mL/min. A temperature program from 60 °C to 300 °C with 5 °C/min and finally 10 min at 300 °C was employed. Mass spectra were recorded in the EI mode with an ionization voltage of 70 eV and a source temperature of 230 °C. The software ChemStation v. F.01.03.2357 (Agilent Technologies, Waldbronn, Germany) for windows was used for data acquisition. Identification of the components was accomplished by comparison of library data (NIST 17) with mass spectral data of commercially purchased standards and diagnostic ions.

To compare the relative abundances of the different compound groups (Extended Data Fig. 6), all compounds were identified (Supplemental Table 8) and grouped either into Alkanes, Alkenes, Alkadienes or Methyl-branched alkanes for each individual.

Antimicrobial assay

To assess the antimicrobial efficacy of MG extracts (Fig. 3d), we quantified the increase over time of the OD in a 96-well plate box, with the outer row filled with 70 µL of PBS. In total we did 3 replicates per sample with a total of 70 µL per sample. Negative control: 70 µL Luria-Bertani (LB) broth (*n*=6). Positive control: 68 µL LB broth + 2 µL *P. aeruginosa* (*n*=6). MG sample: 66 µL LB broth + 2 µL *P. aeruginosa* + 2 µL MG sample (*n*=9).

For the preparation of the pathogen sample, we plated *P. aeruginosa* from a frozen stock on TSA plates. After 24 hours the bacterial culture was replated. After 12 hours aliquots were created using the new bacterial culture in a flask containing 15 mL of freshly sterilized LB

537 broth for an initial OD reading. Afterwards the flask was placed in an incubator shaker (Amerex
538 Steadyshake 757) at 180 rpm, 30 °C for the bacteria to grow. Once the OD readings were
539 between 02-0.5 OD (the exponential growth phase) the flask was put on ice until the
540 experiments started.

541 For the preparation of the MG sample, we pooled 10 MGs in 1.5 mL Eppendorf-Cups. We then
542 froze the samples in liquid nitrogen and crushed the sample material using sterile pellets. We
543 then added 50 µL of PBS-Buffer, vortexed shortly before centrifuging the sample for 5 min at
544 3000 rcf at 4 °C. We then extracted 30 µL of the supernatant into a new cup and repeated the
545 centrifugation process. Afterwards 20 µL of the supernatant was placed again in a new cup and
546 stored at -20 °C. Preparation of the wells was conducted on ice at 4 °C to prevent bacterial
547 growth and degradation of the MG samples. The antimicrobial assays were done in a microplate
548 reader (Synergy H1 BioTek) at 30 °C with a 600 nm wavelength for 8 hours with a double
549 orbital shaking step after each OD reading cycle (every 10 min) at the University of Lausanne.

550 To calculate the intrinsic growth rate of the microbial population (r) in Fig. 3d we used the
551 package growthcurver (v. 0.3.1) with the statistical software R v4.1.0. "r" represents the growth
552 rate that would occur if there were no restrictions imposed on total population size.

553 **Sample collection for metapleural gland extracts**

554 Due to the difficulty of collecting adequate amounts of metapleural gland secretions from the
555 gland's atrium (it is a very sticky substance that adheres to the cuticle), we decided to remove
556 the atrium of the gland together with the secretory cells entirely, using a microscalpel and
557 microscissors. To avoid using a solvent we used a Thermodesorber unit coupled to a GC-MS
558 (TD-GC-MS). For this we transported frozen ants to the University of Würzburg and did the
559 extractions directly in the laboratory next to the TD-GC-MS. One metapleural gland from each
560 of six worker was pooled per sample. As a control we further collected pieces of cuticle of
561 similar size from the side of the thorax to identify any potential contaminations which might
562 have occurred during dissections. In total 3 samples (of 6 individuals each) were analyzed
563 (Extended Data Fig. 8, Supplemental Table 12).

564 **Chemical analysis of the metapleural gland**

565 The MG samples were placed in a glass-wool-packed thermodesorption tube and placed in the
566 thermodesorber unit (TDU; TD100-xr, Markes, Offenbach am Main, Germany). The
567 thermodesorption tube was heated up to 260°C for 10 min. The desorbed components were
568 transferred to the cold trap (5 °C) to focus the analytes using N_2 flow in splitless mode. The

569 cold trap was rapidly heated up to 310 °C at a rate of 60 °C per minute, held for 5 min and
570 connected to the GC-MS (Agilent 7890B GC and 5977 MS, Agilent Technologies, Palo Alto,
571 USA) via a heated transfer line (300 °C). The GC was equipped with an HP-5MS UI capillary
572 column (0.25 mm ID × 30 m; film thickness 0.25 µm, J & W Scientific, Folsom, Ca, USA).
573 Helium was the carrier gas using 1.2874 ml/min flow. The initial GC oven temperature was
574 40 °C for 1 min, then raised at a rate of 5°C per min until reaching 300 °C, where it was held
575 for 3 minutes. The transfer line temperature between GC and MS was 300 °C. The mass
576 spectrometer was operated in electron impact (EI) ionization mode, scanning m/z from 40 to
577 650, at 2.4 scans per second. Chemical compounds were identified using the same protocol as
578 for the CHCs.

579 **Proteomic analysis and sample preparation of the metapleural gland**

580 To characterize the proteins secreted by the metapleural gland, we analyzed the proteome of
581 the atrium of the gland, the metapleural gland secretory cells and the hemolymph (Extended
582 Data Fig. 7). To be considered a metapleural gland protein that could mediate antimicrobial
583 activity, proteins had to be found in the gland's atrium, and must have a higher abundance in
584 the gland's atrium than in the hemolymph. The samples for proteomic analysis were collected
585 in April 2020 from workers of field colonies collected in the Comoé National Park. Three types
586 of samples were collected: Secretory: dissected secretory cells without the atrium, (*n*=6
587 samples, each pooled from five dissections); Hemolymph: hemolymph was collected from the
588 thorax by a glass microcapillary through a small wound (*n*=6 samples, each pooled over five
589 individuals, yielding 4-5 µL); Atrium: due to the difficulty of collecting pure MG content we
590 chose to first widen the opening of the atrium and add 1 µl of PBS before extracting the content
591 together with the PBS (*n*=6 samples, each pooled from five individuals). The samples were
592 kept at -23 °C in Lo-bind Eppendorf tubes with 5µl of PBS together with a 1x Protease inhibitor
593 Cocktail (Sigmafast) during transportation. Once in Lausanne, Switzerland, the samples were
594 kept at -80 °C and processed swiftly.

595 Proteins were digested according to a modified version of the iST protocol[34]. Samples were
596 resuspended in 20 µL of modified iST buffer (1% sodium deoxycholate, 10 mM DTT, 100 mM
597 Tris pH 8.6) and heated at 95 °C for 5 min. They were then diluted with 24 µL of 4 mM $MgCl_2$
598 and 1:100 of benzonase in H_2O and incubated 15 min at ambient temperature. 14 µL of 160
599 mM chloroacetamide (in 10 mM Tris pH 8.6) were then added and cysteines were alkylated
600 for 45 minutes at 25°C in the dark. After addition of 0.5 M EDTA (3 mM final concentration),
601 samples were digested with 0.1 µg of trypsin/Lys-C mix (Promega) at 37 °C for 1 hour,

602 followed by a second enzyme addition (0.1 µg trypsin/LysC) and 1h incubation. Two volumes
603 of isopropanol + 1% trifluoroacetic acid (TFA) were added to one volume of sample and loaded
604 onto an equilibrated OASIS MCX uElution plate (Waters) prefilled with SCX0 buffer (20%
605 MeCN, 0.5% formic acid) and centrifuged. The columns were washed three times with 200 µL
606 isopropanol + 1% TFA and once with 200 µL HPLC solvent A (2% MeCN, 0.1% formic acid).
607 The peptide mixture was then sequentially eluted with 150 µL SCX125 buffer (20% MeCN,
608 0.5% formic acid, 125 mM ammonium acetate), 150 µL SCX500 buffer (20% MeCN, 0.5%
609 formic acid, 500 mM ammonium acetate), and lastly with 150 µL basic elution buffer (80%
610 MeCN, 19% water, 1% NH3).

611 Tryptic peptides fractions were dried and resuspended in 0.05% trifluoroacetic acid, 2% (v/v)
612 acetonitrile, for mass spectrometry analyses. Tryptic peptide mixtures were injected on an
613 Ultimate RSLC 3000 nanoHPLC system (Dionex, Sunnyvale, CA, USA) interfaced to an
614 Orbitrap Fusion Tribrid mass spectrometer (Thermo Scientific, Bremen, Germany). Peptides
615 were loaded onto a trapping microcolumn Acclaim PepMap100 C18 (20 mm x 100 µm ID, 5
616 µm, 100 Å, Thermo Scientific) before separation on a reversed-phase custom packed
617 nanocolumn (75 µm ID × 40 cm, 1.8 µm particles, Reprosil Pur, Dr. Maisch). A flow rate of
618 0.25 µL/min was used with a gradient from 4 to 76% acetonitrile in 0.1% formic acid (total
619 time: 65 min). Full survey scans were performed at a 120'000 resolution, and a top speed
620 precursor selection strategy was applied to maximize acquisition of peptide tandem MS spectra
621 with a maximum cycle time of 0.6 s. HCD fragmentation mode was used at a normalized
622 collision energy of 32%, with a precursor isolation window of 1.6 m/z, and MS/MS spectra
623 were acquired in the ion trap. Peptides selected for MS/MS were excluded from further
624 fragmentation during 60 s.

625 Tandem MS data were processed by the MaxQuant software (version 1.6.14.0)[35] using the
626 Andromeda search engine[36] matching to a custom-made protein database containing 19'618
627 sequences of *M. analis* (July 2019 version, see section "Genome annotation" for details),
628 supplemented with sequences of common contaminants was used. Trypsin (cleavage at K,R)
629 was used as the enzyme definition, allowing 2 missed cleavages. Carbamidomethylation of
630 cysteine was specified as a fixed modification. N-terminal acetylation of protein and oxidation
631 of methionine were specified as variable modifications. All identifications were filtered at 1%
632 FDR at both the peptide and protein levels with default MaxQuant parameters. For protein
633 quantitation the iBAQ values[37] were used. MaxQuant data were further processed with Perseus
634 software (version 1.6.14.0)[38] for filtering, log2-transformation and normalization of values and

635 ortholog annotations. To determine which proteins are secreted by the MG, we proceeded
636 through a series of filters. Proteins not found in the atrium samples were eliminated and those
637 found only in the MG atrium were considered hits. The log2 fold change between the atrium
638 and the hemolymph were determined for all remaining proteins. Only proteins that were on
639 average 1.5-fold more abundant in atrium samples than hemolymph were retained as hits.
640 Percent of total iBAQ per sample was assigned to each protein to indicate abundance.
641 Visualization of heatmaps was performed in Matlab 2020b (clustergram function). To
642 determine whether our selected proteins were toxin-like, we ran clantox[39]
643 (http://www.clantox.cs.huji.ac.il/). Annotations (function, orthology depth and implications for
644 wound healing) found in Supplemental Table 10 were determined using protein BLAST with
645 the experimental clustered nr database[40].

646 The mass spectrometry proteomics data are deposited at the ProteomeXchange Consortium via
647 the PRIDE partner repository with the dataset identifier PXD033003.

648 **Genome sequencing and assembly**

649 The genome of *M. analis* was sequenced and assembled by The Global Ant Genomics Alliance
650 (GAGA, antgenomics.dk)[41]. To identify repeats in the genome assembly, we used the package
651 RepeatModeler v2.0, which combines three *de-novo* repeat finding programs (RECON,
652 RepeatScout and LtrHarvest/Ltr_retriever)[42]. RepeatModeler first probes chunks of the
653 genome assembly to find repeats, then clusters and classifies identified repeats, producing a
654 high-quality library of consensus sequences of repeated sequence families. The consensus
655 sequences were used with RepeatMasker to softmask (in lower-case) all repeats in the genome
656 assembly.

657 **Genome annotation**

658 To annotate the *M. analis* genome assembly we used the *ab-initio* gene predictors Augustus
659 v3.3.3[43] and genemark[44] within the BRAKER2 pipeline v2.1.4[45,46]. Both tools were trained
660 using RNA-seq reads (see below) aligned to the softmasked version of the genome with STAR
661 v2.7[47] and protein evidence from NCBI refseq predictions for *Acromyrmex echinatior, Atta*
662 *colombica, Camponotus floridanus, Dinoponera quadriceps, Linepithema humile,*
663 *Monomorium pharaonis, Ooceraea biroi, Pogonomyrmex barbatus, Solenopsis invicta,*
664 *Temnothorax curvispinosus, Vollenhovia emeryi and Wasmannia auropunctata*. To enable
665 functional interpretation of experimental data, we annotated gene products. First, we identified
666 gene orthologs in *Drosophila melanogaster* to leverage the excellent quality of the functional

667 annotation in this species. To identify the orthologs, we applied a reciprocal best blast approach
668 using Orthologr[48] between the longest protein isoform for each gene from both species[49].
669 Additionally, we identified orthologs with *Apis mellifera* and *Camponotus floridanus* NCBI
670 RefSeq gene annotations. Finally, we ran InterProScan (version 5.30-69.0 and panther-data-
671 14.1) on all proteins using default settings. To assign functional information to *M. analis*
672 annotated genes, we primarily used the gene ontology of *D. melanogaster* orthologs, but also
673 results from sequence homology search on Interproscan and the Uniprot database.

674 To study the effect of infections on gene expression (Extended Data Fig. 7), we conducted a
675 transcriptomic analysis. We dissected the gaster from the same infected (soil OD=0.1, *n*=20)
676 and sterile ants (*n*=20), whose thorax were used for the microbiome analyses in Fig. 1AB.
677 Samples were collected 2 and 11 hours after manipulation (*n*=10 per timepoint) in the Comoé
678 field research station and had the sting together with the venom reservoir removed. The gaster
679 was dissected without solvent and stored in a RNAlater stabilisation solution at -23 °C
680 (ThermoFisher Scientific) for later analyses at the University of Lausanne. Afterwards, the
681 samples were homogenized with ceramic beads in 1ml of Trizol reagent. Homogenized
682 samples were incubated for 5 min at room temperature (RT) in Trizol, before adding
683 Chloroform (200 µL). Samples were incubated for 5 min at RT then centrifuged (25 s at 12,000
684 rpm and 4 °C) and the upper aqueous layer (~500 µL) transferred to a new tube. We added
685 Isopropanol (650 µL) and Glycogen blue (1 µL; RNAse-free, Invitrogen, 15 mg/mL,
686 #AM9516) then vortexed and incubated overnight at -20 °C. To purify the RNA, we used a
687 EtoH precipitation method: samples were centrifuged (30 s at full speed at 4 °C), the
688 supernatant was discarded and EtOH (1 mL at 80%) added. We repeated this step a second
689 time with EtOH (1 mL at 70%). Finally, the supernatant was removed and the pellet, after a
690 brief air dry (15-20 s) at RT, was resuspended in nuclease-free water. Libraries were prepared
691 with the KAPA Stranded mRNASeq Library Preparation Kit (#KK8421) according to the
692 manufacturer's protocol. Paired end sequencing was performed on an Illumina Hiseq4000
693 sequencer at the Genomic Technology Facility of the University of Lausanne. We obtained
694 ~15-25 million PE reads per individual. Sequence reads have been deposited in NCBI Sequence
695 Read Archive (SRA) under the accession number PRJNA823913.

696 We mapped RNA-seq reads on the softmask genome assembly using STAR v2.7 with the 2-
697 pass mapping option and using the gene annotations to properly find exonic junctions[47]. Then,
698 we used the program featureCounts from the Subread package to count the number of reads
699 mapped on each exon for each gene[50]. Then using the count's files, we performed differential

700 gene expression analyses using DESeq2[51] of sterile and infected workers collected at 2 and 11
701 hours after treatment. *P* values of differential expression analyses were corrected for multiple
702 testing with a false discover rate (FDR) of 5%.

703 **X-Ray Micro-CT imaging**

704 To examine the internal morphology of the MG (Fig. 3a), we scanned and visualized an
705 intermediate sized worker (CASENT0744096), although multiple other workers of different
706 sizes were scanned and visually inspected to confirm the morphology of the exemplar specimen
707 was representative. The specimens were fixed in 90% ethanol, stained in 2 M iodine solution
708 for a minimum of 7 days, then washed and sealed in a pipette tip with 99% ethanol for scanning.
709 The scans were performed with the ZEISS Xradia 510 Versa 3D X-ray microscope at the
710 Okinawa Institute of Science and Technology Graduate University, Japan. We scanned the
711 thorax (mesosoma) and whole body to visualize both the structure of the gland, and its location
712 in the whole ant. The scan parameters for the thorax scan were: Voxel size, 4.404 µm; Exposure
713 time, 6 s; Voltage, 40 kV; Power, 3 W; Source distance, 23.147 mm; Objective, 4x;
714 Projections, 1601. For the full body scan, we used: Voxel size, 12.5 µm; Exposure time, 1 s;
715 Voltage, 40 kV; Power, 3 W; Source distance, 25.03 mm; Objective, 0.4x; Projections, 1601.
716 The 3D reconstruction was performed using the ZEISS Scout-and-Scan Control System
717 Reconstructor software (ZEISS Microscopy, Jena, Germany). The MG structures were
718 manually segmented using Amira (version 2019.2; Thermo Fisher Scientific, Berlin, Germany)
719 and visualized using VGStudio3.4 (Volume Graphics GmbH, Heidelberg, Germany). The
720 gland atrium was rendered using isosurface and a clipping plane was created to visualize the
721 cross-section. All other materials were visualized using Phong volume rendering.

722 **Statistical analysis**

723 For statistical analyses and graphical illustration, we used the statistical software R v4.1.0[52]
724 with the user interface RStudio v1.4.1717 and the R package ggplot2 v3.3.5[53]. To select the
725 appropriate statistical tests, we tested for deviations from the normal distribution with the
726 Shapiro Wilks test ($P>0.05$). A Bartlett test was used to verify homoscedasticity ($P>0.05$). All
727 our models included colony as a random factor and an overall likelihood ratio test against an
728 intercept only model. In case of multiple testing, a Holm-Bonferroni correction was performed
729 with the adjusted P-values given throughout the text. To test for significant differences in the
730 survival curves, we conducted mixed effect cox proportional hazards regression models
731 (Extended Data Fig. 2) using the R package survminer (v0.4.9) followed by post-hoc analyses

732 using least square means with the R package lsmeans (v.2.30; Supplemental Table 2, 3 & 5).
733 The survival curves were illustrated using Kaplan-Meier cumulative survival curves (Fig. 1c,
734 2a, 4, Extended Data Fig. 3 & 5). For the bacterial load (ΔCq) within the thorax content between
735 treated and untreated infected individuals (Fig. 1a & 2b) we conducted linear mixed effect
736 models with a least square means (lsmeans) post-hoc analysis. For the bacterial growth
737 inhibition (Fig. 3d) we conducted Mann-a Whitney U test. Differences in the CHC-profile
738 composition were calculated using a permutational multivariate analysis of variance
739 (ADONIS) on a Bray-Curtis dissimilarity matrix using the package vegan (v.2.5-7;
740 Supplemental Table 7). For the different durations of MG care between sterile and infected
741 individuals (Extended Data Fig. 4), we conducted a linear mixed effect model with individual
742 as random factor followed by a Satterthwaite's t-test. For differences between chemical
743 compound groups of the CHC profiles (Extended Data Fig. 5), we conducted an analysis of
744 variance (AOV) followed by a Tukey Honest Significant differences test (Supplemental Table
745 9). For behavioral differences in wound care between sterile and infected individuals (Fig 3b,
746 c), we modeled wound care as a binary event using binomial generalized additive models with
747 posthoc contrasts to identify intervals of time during which the probability of receiving wound
748 care differed between sterile and infected individuals. See Supplemental Information for a
749 reproducible modeling workflow.

750 **Data and materials availability**

751 Raw amplicon-sequence data was deposited at the Sequence Read Archive (SRA) under
752 PRJNA826317. Sequence reads were deposited in NCBI Sequence Read Archive (SRA) under
753 the accession number PRJNA823913. The proteomics data was deposited at the
754 ProteomeXchange Consortium via the PRIDE partner repository with the dataset identifier
755 PXD033003. The remaining data is available in the Dryad Digital Repository:
756 https://doi.org/10.5061/dryad.hqbzkh1j6

Methods references

25. Konaté, S. & Kampmann, D. *Biodiversity atlas of West Africa, Volume 3: Côte d'Ivoire*. (Abidjan & Frankfurt am Main, 2010).
26. Schmidt, C. A. & Shattuck, S. O. The Higher Classification of the Ant Subfamily Ponerinae (Hymenoptera: Formicidae), with a Review of Ponerine Ecology and Behavior. *Zootaxa* **3817**, 1-242 (2014).
27. Villet, M. H. Division-of-Labor in the Matabele Ant *Megaponera foetens* (Fabr) (Hymenoptera-Formicidae). *Ethol Ecol Evol* **2**, 397-417 (1990).
28. Looke, M., Kristjuhan, K. & Kristjuhan, A. Extraction of genomic DNA from yeasts for PCR-based applications. *Biotechniques* **50**, 325-328 (2011).
29. Schoch, C. L. *et al.*, Nuclear ribosomal internal transcribed spacer (ITS) region as a universal DNA barcode marker for Fungi. *Proc Natl Acad Sci USA* **109**, 6241-6246 (2012).
30. Boratyn, G.M., Thierry-Mieg, J., Thierry-Mieg, D., Busby, B. & Madden, T.L. Magic-BLAST, an accurate RNA-seq aligner for long and short reads. *BMC Bioinform* **20**, 405 (2019).
31. Kešnerová, L. *et al.*, Disentangling metabolic functions of bacteria in the honey bee gut. *PLoS Biol* **15**, e2003467 (2017).
32. Gallup, J.M. "qPCR inhibition and amplification of difficult templates." in *PCR troubleshooting and optimization: the essential guide*. S. Kennedy, N. Oswald, Eds (Caister Academic Press, 2011), chap.2.
33. Kešnerová L. *et al.*, Gut microbiota structure differs between honeybees in winter and summer. *ISME J* **14**, 801-814 (2020).
34. Kulak, N. A., Pichler, G., Paron, I., Nagaraj, N. & Mann, M. Minimal, encapsulated proteomic-sample processing applied to copy-number estimation in eukaryotic cells. *Nat Methods* **11**, 319-324 (2014).
35. Cox, J & Mann, M. MaxQuant enables high peptide identification rates, individualized p.p.b.-range mass accuracies and proteome-wide protein quantification. *Nat Biotechnol* **26**, 1367-1372 (2008).
36. Cox J. *et al.*, Andromeda: A Peptide Search Engine Integrated into the MaxQuant Environment. *J Proteome Res* **10**, 1794-1805 (2011).
37. Schwanhausser B. *et al.*, Global quantification of mammalian gene expression control. *Nature* **473**, 337-342 (2011).
38. Tyanova S. *et al.*, The Perseus computational platform for comprehensive analysis of (prote)omics data. *Nat Methods* **13**, 731-740 (2016).
39. Naamati, G., Askenazi, M. & Linial, M., ClanTox: a classifier of short animal toxins. *Nucleic Acids Res* **37**, 363-368 (2009).
40. Steinegger, M. & Söding, J. MMseqs2 enables sensitive protein sequence searching for the analysis of massive data sets. *Nat Biotechnol* **35**, 1026–1028 (2017).
41. Boomsma J.J. *et al.*, The Global Ant Genomics Alliance (GAGA). *Myrmecological News* **25**, 61-66 (2017).
42. Flynn, J. M. *et al.*, RepeatModeler2 for automated genomic discovery of transposable element families. *Proc Natl Acad Sci USA* **117**, 9451-9457 (2020).
43. Stanke, M., Diekhans, M., Baertsch, R. & Haussler, D. Using native and syntenically mapped cDNA alignments to improve de novo gene finding. *Bioinformatics* **24**, 637-644 (2008).
44. Lomsadze, A., Ter-Hovhannisyan, V., Chernoff, Y. O. & Borodovsky, M. Gene identification in novel eukaryotic genomes by self-training algorithm. *Nucleic Acids Res* **33**, 6494-6506 (2005).
45. Hoff, K. J., Lange, S., Lomsadze, A., Borodovsky, M. & Stanke, M. BRAKER1: Unsupervised RNA-Seq-Based Genome Annotation with GeneMark-ET and AUGUSTUS. *Bioinformatics* **32**, 767-769 (2016).
46. Bruna, T., Hoff, K. J., Lomsadze, A., Stanke, M. & Borodovsky, M. BRAKER2: automatic eukaryotic genome annotation with GeneMark-EP+ and AUGUSTUS supported by a protein database. *NAR Genom Bioinform* **3**, lqaa108 (2021).
47. Dobin A. *et al.*, STAR: ultrafast universal RNA-seq aligner. *Bioinformatics* **29**, 15-21 (2013).
48. Drost, H. G., Gabel, A., Grosse, I. & Quint, M. Evidence for Active Maintenance of Phylotranscriptomic Hourglass Patterns in Animal and Plant Embryogenesis. *Mol Biol Evol* **32**, 1221-1231 (2015).
49. Altschul, S. F., Gish, W., Miller, W., Myers, E. W. & Lipman, D. J. Basic Local Alignment Search Tool. *J Mol Biol* **215**, 403-410 (1990).
50. Liao, Y., Smyth, G. K. & Shi, W. featureCounts: an efficient general purpose program for assigning sequence reads to genomic features. *Bioinformatics* **30**, 923-930 (2014).
51. Love, M. I., Huber, W. & Anders, S. Moderated estimation of fold change and dispersion for RNA-seq data with DESeq2. *Genome Biol* **15**, (2014).
52. R Core Team. (R Foundation for Statistical Computing, Vienna, Austria, 2013).
53. Wickham, H. *ggplot2: Elegant Graphics for Data Analysis*. (Springer-Verlag New York, 2009).

End notes

Acknowledgments

We thank the Comoé National Park Research Station for the use of their facilities for the field and laboratory research and the park management of Office Ivoirien des Parcs et Réserves for facilitating field research in the park. We thank GAGA for providing the assembled *Megaponera analis* genome. We thank Barbara Milutinovic and the Cremer lab at IST Austria for teaching us the methodology for the antimicrobial assay. We thank Christine La Mendola for her help with sample preparation for genetic analyses and Camille Lavoix for proof reading of the manuscript. This study was supported by the Swiss NSF and an ERC grant to LaK. ACL was supported by Swiss SNSF grant PR00P3_179776. ETF was also supported by the DFG Emmy Noether Programme (n°: 511474012).

Author contributions:

Conceptualization: ETF, LaK

Methodology: ETF, LuK, JL, QH, ACL, AD, FA, EPE, PW, TS, DBS

Investigation: ETF, LuK, JL, QH, ACL, EPE, TS

Visualization: ETF, QH, FA, EPE, ACL, JL, DBS

Funding acquisition: LaK

Project administration: ETF, PE, LaK

Supervision: ETF, LaK

Writing – original draft: ETF, LaK

Writing – review & editing: ETF, LuK, JL, QH, ACL, AD, FA, EPE, PW, PE, TS, DBS, LaK

Competing interests: Authors declare that they have no competing interests.

Additional information: Supplementary information is available for this paper.

Correspondence and requests for materials should be addressed to Erik T. Frank.

Extended Data

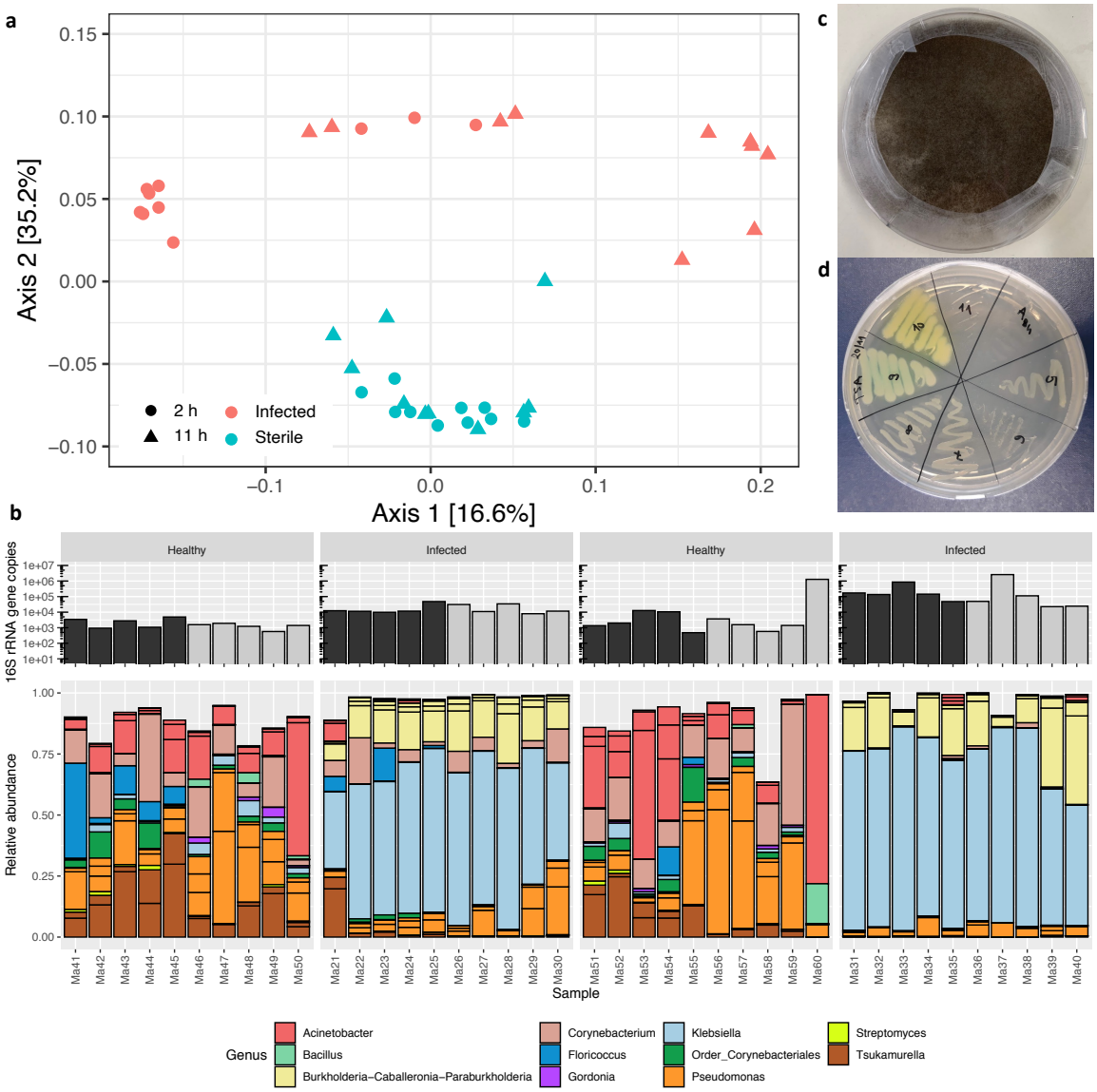

Extended Data Fig. 1 | Ant microbiome and soil pathogens. (a) Principal Coordinate Analysis of the microbiome of the thorax of sterile and infected ants at 2 and 11 hours (as seen in Fig. 1b). ADONIS: Treatment: F=17.451; R^2=0.31; P<0.001. **(b)** 16S rRNA gene copy numbers and relative abundance of bacterial genera present in the thorax of the same individuals as in Fig. 1A. Multiple bars of the same color indicate different amplicon-sequence variants (ASVs) belonging to the same genera. ADONIS: Treatment: F=17.45; R^2=0.31; P<0.001 **(c)** Microbial culture of surface soil grown on an agar plate (mostly showing fungal mycelia of *Rhizopus* with black spores). **(d)** Bacterial cultures of isolated *Pseudomonas aeruginosa* strains from the soil.

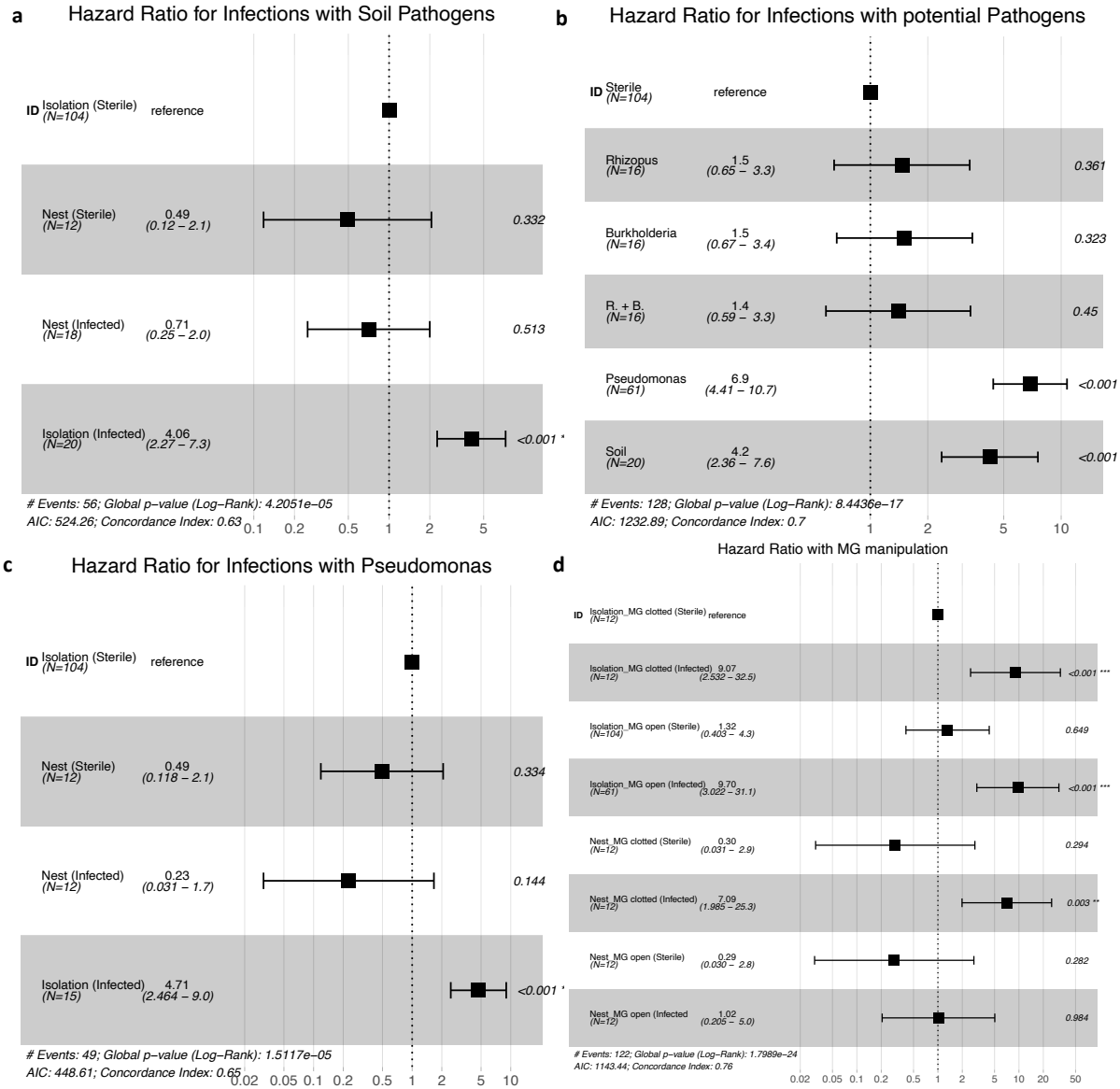

Extended Data Fig. 2 | Cox proportional hazard models for survival of infections. The reference were sterile ants in isolation with colony of origin as random factor. **(a)** Statistical results for infected ants (surface soil pathogens: OD=0.1) in isolation and inside the nest (Fig. 1c). **(b)** Statistical results for infected ants kept in isolation exposed to different potential pathogens cultured from the soil (*Burkholderia*, *Rhizopus*, *Pseudomonas*; OD=0.1) or surface soil pathogens (Extended Data Fig. 3). **(c)** Statistical results for infected and sterile ants (*P. aeruginosa*: OD=0.05) in isolation and with nestmates in the nest (Fig. 2a). **(d)** Statistical results of infected ants (*P. aeruginosa*: OD=0.05) kept in isolation or inside sub-colonies containing workers with or without plugged MG openings (Fig. 4; Extended Data Fig. 5).

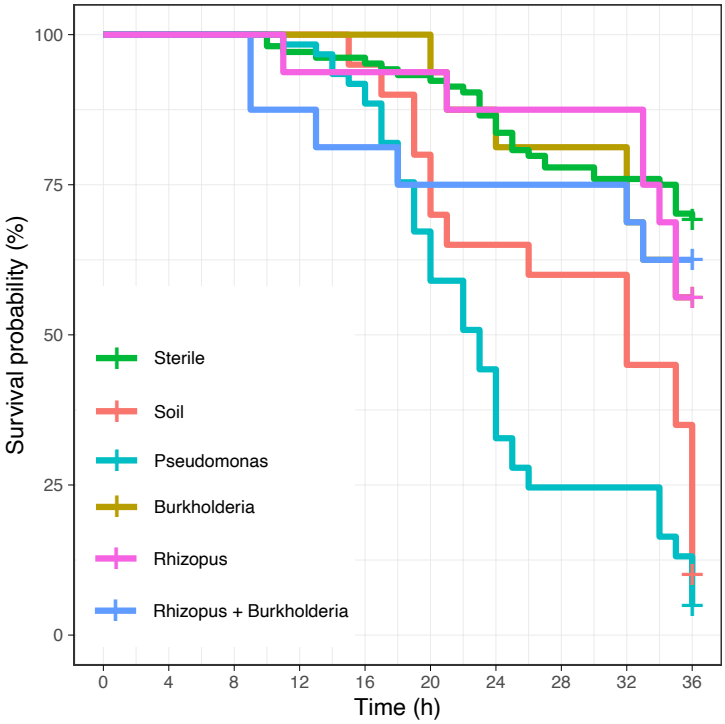

Extended Data Fig. 3 | Survival probability for different pathogen types. Kaplan – Meier cumulative survival rates of workers kept in isolation chambers. All individuals had one hind leg cut off at the femur, the wound was then exposed to a sterile PBS solution (Sterile, *n*=104), a mix of either surface soil pathogens (Soil OD=0.5, *n*=20) or isolated pathogens diluted in PBS (OD=0.1): *P. aeruginosa* (*Pseudomonas*, *n*=61), *Burkholderia* (*n*=16), *Rhizopus* (*n*=16), or *Rhizopus* with *Burkholderia* (*n*=16). The treated ants were observed for 36 hours and the time of death noted. Statistical significance tested with a mixed-effects Cox proportional hazards regression model (Extended Data Fig. 2b).

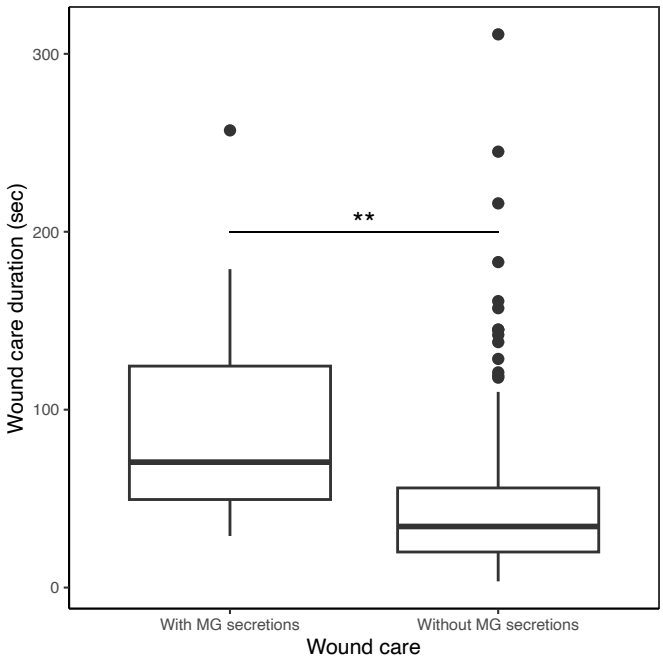

870

871 **Extended Data Fig. 4 | Differences in wound care duration with and without metapleural gland**
872 **secretions.** Duration of wound care with and without MG secretions for the first 24 hours after injury
873 inside the nest. With MG secretions: wound care involving the MG for both infected and sterile ants
874 pooled together using either the MG of the injured ant (*n*=26 for infected, *n*=10 for sterile ants) or of
875 the nursing ant (*n*=2 for infected, *n*=4 for sterile ants), total sample size *n*=42. Without MG secretions:
876 wound care excluding the MG for both infected and sterile ants pooled together (*n*=174 for infected,
877 *n*=192 for sterile ants), total sample size *n*=366. Linear mixed effect model (Random Factor: Individual:
878 Variance=134.4, Std. Dev.=11.59; Residual: Variance=2671.2, Std. Dev.=51.68) with Satterthwaite's t-test
879 for wound care duration with and withut MG secretions: t=-3.09; *P*=0.003**.

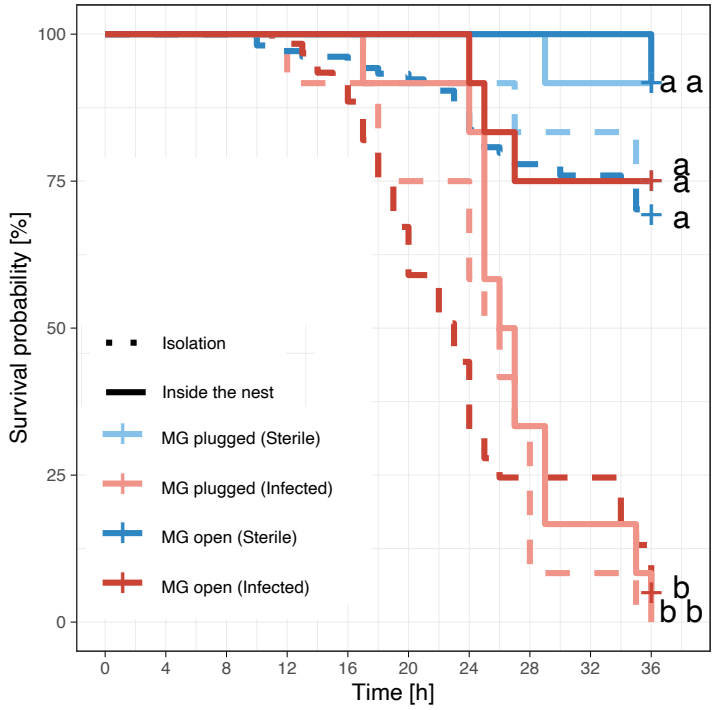

Extended Data Fig. 5 | Importance of MG secretions on survival of sterile and infected ants. Kaplan – Meier cumulative survival rates of workers in isolation (dotted line) or inside sub-colonies (solid line) whose wounds were exposed to *P. aeruginosa* diluted in PBS (Infected, OD=0.05) or a sterile PBS solution (Sterile). In three sub-colonies all ants had their MG opening closed with acrylic color (MG plugged), while it remained open in the other three sub-colonies (MG open). *n*=12 per treatment. Detailed statistical results in Extended Data Fig. 2d and Supplemental Table 5.

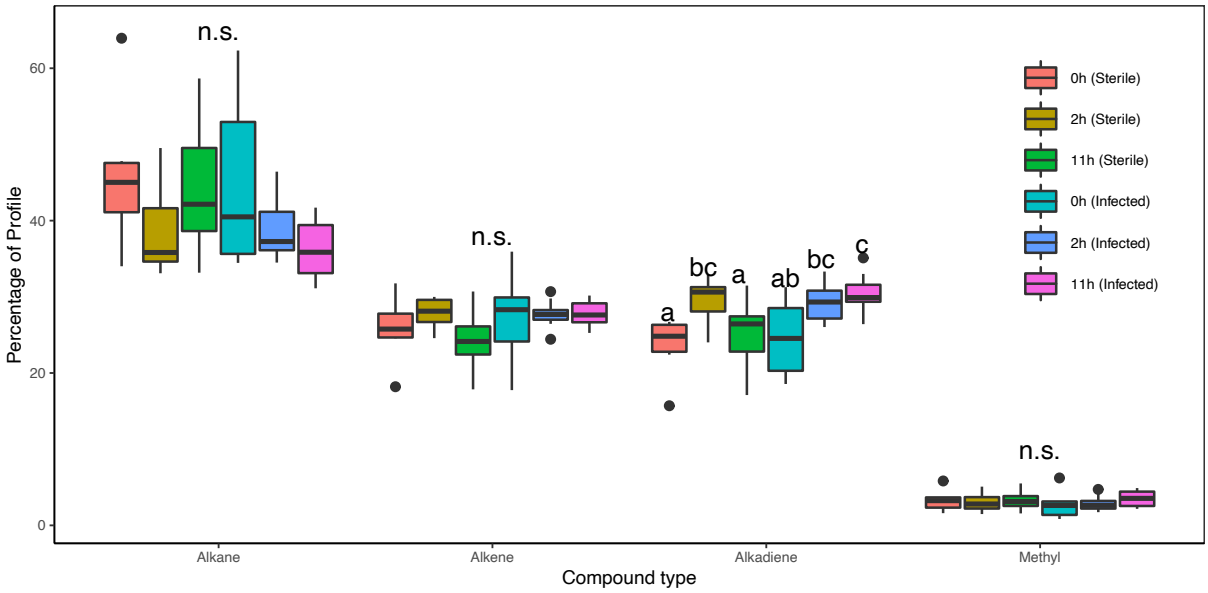

887

888 **Extended Data Fig. 6 | Chemical composition of cuticular hydrocarbon profiles of sterile and infected**
889 **ants.** Differences across compound types (alkanes, alkenes, alkadienes and methyl-branched alkanes) for
890 sterile ants (Sterile; *n*=30) and ants infected with *P. aeruginosa* diluted in PBS (OD=0.05, Infected; *n*=30)
891 at three different time points (0, 2 and 11 hours). Detailed statistical results in Supplemental Table 8.

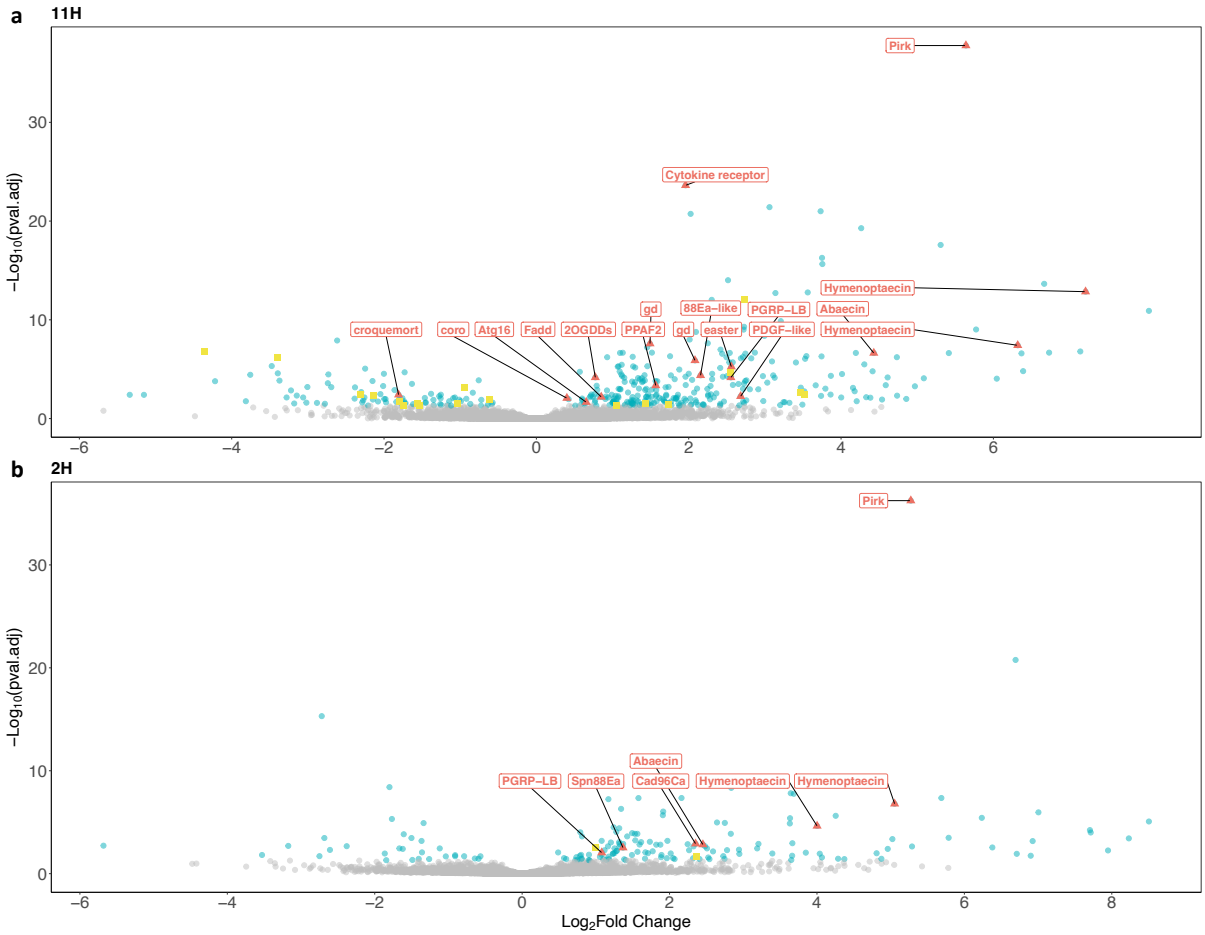

892

893 **Extended Data Fig. 7 | Differential gene expression between sterile and infected ants 2 and 11 hours**
894 **after injury.** Infection triggers changes in the expression of hundreds of genes. Volcano plot illustrates the
895 fold up- and down-regulation of immune-related genes (red triangles, Supplemental Table 10) and lipids and
896 CHC-related genes (yellow squares, Supplemental Table 9), 11 hours **(a)** and 2 hours **(b)** after infection.
897 Positive Log2FoldChange values correspond to genes up-regulated in infected ants when compared to sterile
898 ants, while negative values are down-regulated in infected ants. *P*-values are corrected for multiple testing
899 using the Benjamini and Hochberg method (genes with significant differential expression marked in blue,
900 i.e. adjusted *P*-value <0.05).

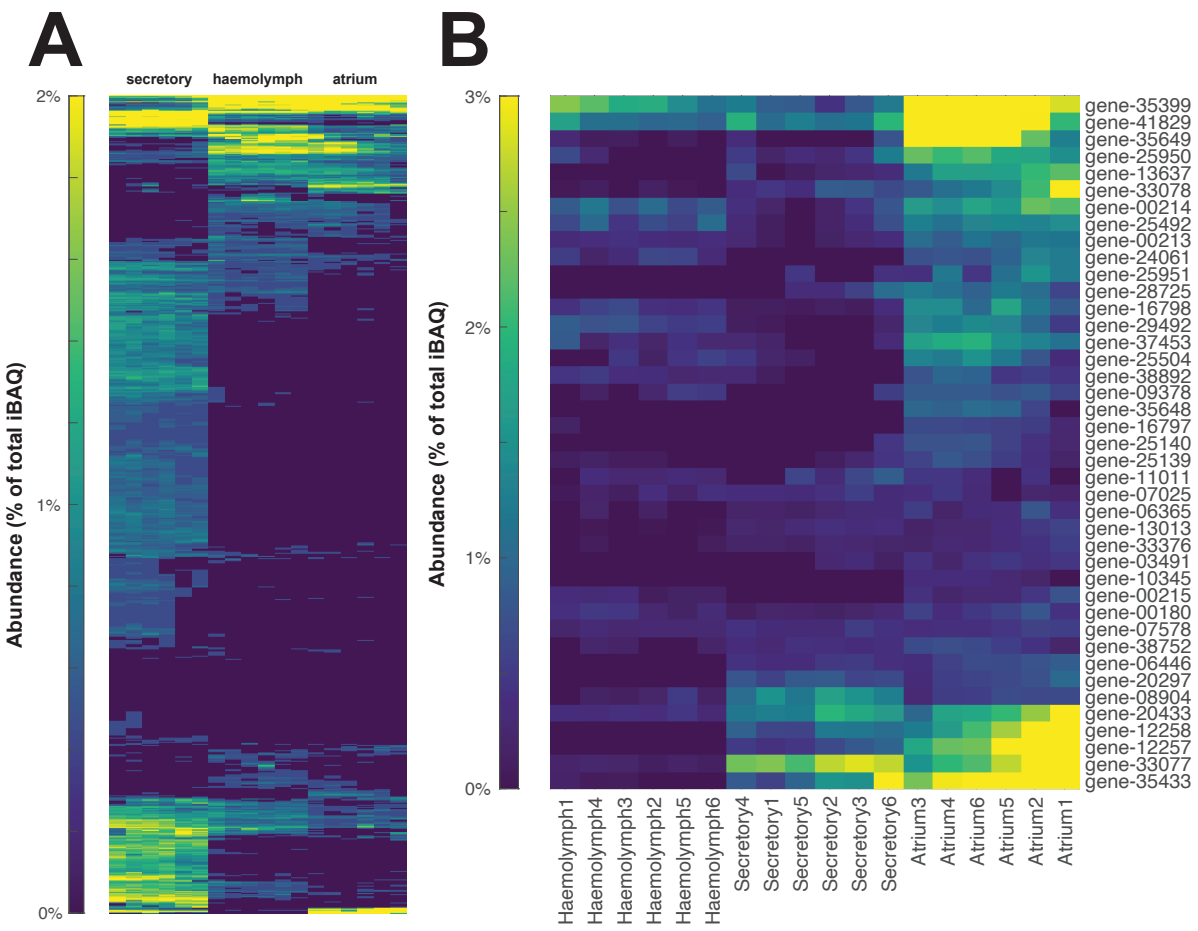

Extended Data Fig. 8 | Proteins from the metapleural gland. (a) All proteins identified in hemolymph (*n*=6), secretory cells (*n*=6) and metapleural gland atria (*n*=6). **(b)** The 41 proteins deduced through filtering to be secreted by the metapleural gland. Gene annotations can be found in Supplemental Table 11. Heatmap colors indicate normalized percentages of total iBAQ for a given sample.

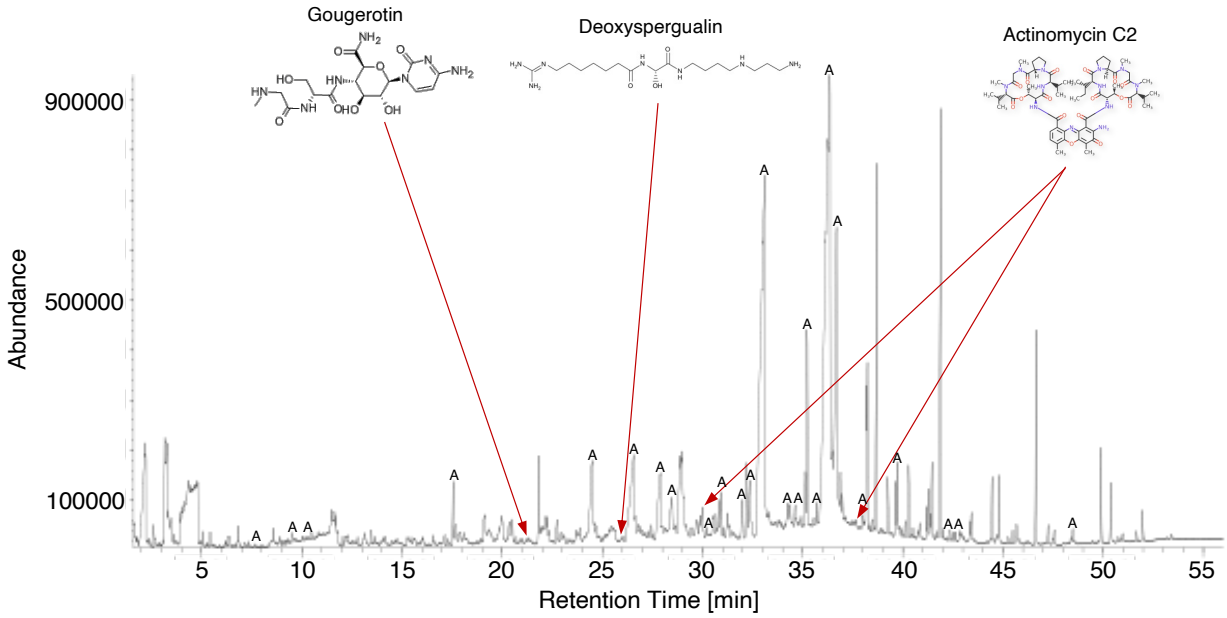

Extended Data Fig. 9 | Chemical compounds in the metapleural gland. Gas-chromatographic representation of one sample of 6 pooled metapleural glands. Red arrows indicate chemical compounds with similar structure to known antibiotics and antimicrobials. Peaks marked with the letter A represent carboxylic acids. A detailed list of all chemical compounds found in the MG is described in Supplemental Table 12.

Supplemental Materials

Supplemental Tables 1 to 13

Supplemental Model Workflow

Supplemental Movies 1 to 2